

We thank the referees for their careful and critical review of our paper. The following are our responses to the referees' comments.

Response to Anonymous Referee #1

In the manuscript the authors measured several physicochemical properties, including size, density, chemical composition, hygroscopicity, and Cloud Condensation Nuclei (CCN) activity of coated Black Carbon (BC) particles as a function of aging (coating with condensable species from photo-oxidation of VOCs) in a quasi-atmospheric aerosol evolution study (QUALITY) chamber using a suite of instruments, such as differential mobility analyzer, aerosol particle mass analyzer, High Resolution – Time of Flight – Aerosol Mass Spectrometer (HR-ToF-AMS), Humidified Tandem Differential Mobility Analyzer (HTDMA), and a CCN Counter (CCNC). Their results show that under ambient condition in Beijing, the BC undergoes rapid growth to 77 ± 33 nm coating thickness with an average growth rate of 26 ± 11 nm h⁻¹. The O/C ratio of the SOA coating is 0.5, lower than ambient level, indicating the lack of aqueous phase oxidation inside QUALITY chamber. The hygroscopic parameter is about 0.035 - 0.040 as measured by HTDMA and CCNC, suggesting that the initial photochemical aging of BC particles does not appreciably alter the particle hygroscopicity in Beijing. This study and the data provided are quite extensive. The most valuable addition of this manuscript is the “close to ambient (Beijing)” aging condition in the QUALITY chamber. The author showed in Figure 3 that the O₃, NO_x, CO, and SO₂ concentrations inside and outside of the chamber is close. However, the VOCs plot inside and outside of the chamber is missing. The authors also mentioned they applied heater, drier, alumina spherules coated with potassium permanganate (KMnO₄), and activated charcoal to remove the VOCs, H₂S, SO₂, NO_x, and O₃. It would be nice if the authors could also show the VOCs are efficiently removed down to sub-ppb level while injecting the BC particles into the chamber. Did the authors use proton-transfer-reaction mass spectrometer (PTR-MS) to monitor the VOCs inside and outside the chamber? Since the coating is caused by condensable species from photo-oxidation of VOCs and “close to ambient” condition is an important part of the manuscript, I would suggest the authors add the VOC plot.

We thank the reviewer very much for the insight suggestion. We have added another figure (as Figure 3 in current version), which demonstrates the comparison of VOCs concentration between chamber and ambient air before the BC aging experiment. Corresponding discussion is also added in the text as (Line 231):

“To investigate the VOCs concentration inside the reaction chamber after the injection of BC particles, both the chamber and ambient air were sampled with VOC canisters just before the BC aging experiment started. These canisters were then analyzed by a gas chromatography-mass spectrometer / flame ionization detector (GC-MS/FID, HP inc.) system (Liu et al., 2008). The concentrations of VOCs containing 4 or more carbons are illustrated in Figure 3. Slightly higher concentrations of several VOCs in the QUALITY chamber, e.g., n-butane, n-pentane, toluene, were observed compared with those in the ambient air, duo to the co-injection of a small amount of VOCs together with BC particles into the chamber. Nevertheless, the average increase of the VOC concentrations was only 16% or 0.1 ppb for all focused VOCs species, with the largest increase of 35% or 0.36 ppb, suggesting the insignificant influence of soot burner on VOCs concentrations and SOA formation in the chamber.”

Besides my major point above, I also have several minor comments.

1) On page 1 in abstract (line 18), “wall loss of primary gaseous pollutants was negligible, : : :”, please add “was negligible compared with the replenish rate by gas exchange”. Because other readers who don’t have gas exchange might also think it is negligible in their chamber, which will cause confusion.

We thank the reviewer for this suggestion. The sentence has been modified as suggested.

2) On page 3 (line 100), is “polytetrafluoroethylene” PTFE? PFA should be “Perfluoroalkoxy alkane”.

We are sorry for such mistake. The “polytetrafluoroethylene” should be “Perfluoroalkoxy alkane”. It has been revised in the manuscript.

3) On page 6 (line 207), “The transmission : : : were measured using a Fourier Transform Infrared Spectroscopy (FTIR) system”. However, in the following context, the authors are discussing about the UV-Vis spectrum of the Teflon film and acrylic shell. Did I miss something? Or does the authors actually mean “UV-Vis” system?

We thank the author for pointing out his mistake. The sentence has been revised as “The transmission efficiencies of each material were measured using an ultraviolet-visible (UV-Vis) spectrophotometry (PerkinElmer Inc., model 552).”

4) On page 12 (line 444), Fig. 11a and Fig. 11b should be Figure 10a and Figure 10b. Please correct that.

It has been revised. Thanks.

5) On page 13 (line 473, and equation 3), if some of SOA components are not very soluble in water, the updated formula in reference (Petters and Kreidenweis 2008) (formula 10) should be used. Otherwise, based on the kappa of 0.04, the average molecular weight of the coating material is about 450 g mol⁻¹.

We agree with the reviewer that the updated formula in reference (Petters and Kreidenweis 2008) (formula 10) is more accurate to calculation the kappa value when coating material is not highly hygroscopic. However, the calculation requires the solubility of SOA, which is impossible to be obtained duo to the variable VOC precursors and complex photochemical reactions in the ambient condition. Nevertheless, we added discussion on the uncertainty to use of this mixing rule as “Since the SOA formed inside the chamber was not highly hygroscopic, some of the SOA components might not be able to solve in water droplets (Petters and Kreidenweis, 2008), lead to the underestimation of the κ values of the coating materials in this study.”

6) This is not a comment but a discussion. In the end of “Section 4”, the authors discussed about the

relationship between κ and O/C ratio. In the reference (Jimenez et al. 2009), Figure 3 shows at around O/C = 0.5, the κ is about 0.12 for ambient (including Mexico City, Jungfraujoch, Hyytilala SV-OOA, Hyytilala LV-OOA) and α -pinene SOA, but about 0.16 for Trimethylbenzene (TMB) SOA. All the cases have larger κ values than reported here (0.04). However, in another reference (Massoli et al. 2010), Figure 2 shows the α -pinene and m-xylene SOAs have κ value about 0.14 at O/C=0.5, but TMB SOA has κ value of only 0.04, consistent with the value (0.04) reported here. If we believe the latter reference is correct, does that mean the VOC source in Beijing is more TMB like? O/C could not be used as the only parameter for predicting κ as discussed. This could also suggest the VOC source in Beijing is different from other places, such as Mexico City.

The reviewer made a very interesting point to examine the application of this study. However, we don't have enough evidence to draw such conclusion yet. First, "The O/C ratio of the coating SOA is 0.5 in our experiment, corresponding to the O/C ratio of approximately 0.4 in Jimenez et al. (2009) and Massoli et al. (2010) due to the utilization of updated AMS calibration method in this study." The κ value at O/C=0.4 will be lower than that provided above by the reviewer. Second, the κ_{HGF} of α -pinene and α -pinene/xylene mixture is consistent with our κ_{HGF} at same O/C ratio. Third, in the measurements at other sites around the world, e.g., Mexico City, Jungfraujoch, Hyytilala, the measured κ value of organics were for the total OM in the atmosphere, including both primary and secondary OM with different aging degree (from hours to days) through both photochemical and heterogeneous pathways. In this study, however, the SOA is mainly from photochemical reactions with aging time scale of only a few hours. Therefore, we can't conclude that the SOA hygroscopicity in Beijing is different from other cities at the moment. But we believe that this is an interesting aspect and we would like to focus this in our future studies.

Response to Anonymous Referee #2

The manuscript investigated the changes in the hygroscopicity of elemental carbon (EC) aerosol during aging in QUALITY chamber where the gaseous species in ambient air constantly diffused into the reaction chamber and products from their photochemical reactions interacted with mono-dispersed EC seed particles. The variations in EC particle size, mass, chemical composition, hygroscopicity and CCN properties were monitored throughout the aging processes. This study provides a unique perspective among chamber studies because the EC seed aerosol was exposed to photochemical oxidation products from an environment that closely mimics the actual ambient air. Evaluating the hygroscopicity of EC has been a challenge for the atmospheric sciences research community due to the complex morphology changes. Following the method of using mono-dispersed seed aerosol (Qiu et al. ES&T, 2012 and Khalizov et al. ES&T, 2013), this study provided new insights into this complex research problem. The current manuscript also nicely supplements a recent publication from the same authors (Peng et al. PNAS, 2016) by providing detailed evaluation of the the QUALITY chamber. The characterization of the QUALITY chamber experiments appeared to be thorough and the results appeared to be reliable. The topic is relevant to the scope of the journal of Atmospheric Chemistry and Physics and should be considered for publication. A few comments are provided to facilitate the further improvement of the manuscript:

(1) Recent studies showed (for example, Chen et al. Geophys. Res. Lett. 2016, 43, 11080) that the morphology of nascent EC particles can be highly sensitive to even a small change in the organic coating on the primary spheres. As a result, it is prudent to provide experimental data to show that all the EC seed particles started with similar morphology and chemical composition. What was the thickness (or weight percent) of volatile organics in the seed particles at the beginning of each chamber aging experiment?

We thank the reviewer for the suggestion. In our study, the fresh BC particles were highly fractal. For three initial mobility diameters (D_m) of about 100 nm, 150 nm, and 200 nm, the ranges of effective density for fresh BC particles in each experiment are 0.43-0.50 g cm⁻³, 0.34-0.34 g cm⁻³, and 0.24-0.32 g cm⁻³, respectively (Table 2 of the manuscript). Accordingly, the dynamic shape factors (DSF) of 100 nm, 150 nm, and 200 nm BC particle are 2.11-2.30, 2.54-2.55 and 2.44-2.85, respectively. This suggests the highly fractal morphology of the fresh BC particles, and the consistency of fresh BC properties in different experiment. Also, as the BC particles formed from the burner were heated to 300 °C before introduced into the chamber, most of the organic coatings were removed. The combined measurement of particle size distribution, density and chemical composition (AMS) shows that organics accounted for less than 10% of fresh BC mass concentration. The single scattering albedo (SSA) of fresh BC particles was only 0.1, further confirming the purity of BC particles. We modified two places in the manuscript to make this clear:

Line 132, “The combined measurement of particle size distribution, density and chemical composition exhibited that organics accounted for less than 10% of fresh BC mass concentration. Moreover, the single scattering albedo (SSA) of fresh BC particles was only 0.1, further confirming that few organic coatings existed on fresh BC particles.”

Line 238, “For three initial D_m of 100 nm, 150 nm, and 200 nm, the ranges of effective density of fresh BC particles in each experiment were 0.43-0.50 g cm⁻³, 0.34-0.34 g cm⁻³, and 0.24-0.32 g cm⁻³, respectively, indicating highly fractal BC aggregates (Zhang et al., 2008).

The small variation for particles with the same D_m also demonstrates the consistency of fresh BC morphology in different experiments.”

(2) *Evaluating the hygroscopic changes of EC has been a challenge. It has been proposed (for example, Qiu et al. ES&T, 2012) that the hygroscopicity of the coating materials can be measured or estimated to reflect the real hygroscopic growth of the EC particles. The authors may consider incorporating such approach to convert the apparent HGF into the real HGF. Furthermore, I wonder if similar approach can be developed for the CCN data to estimate the real κ values of aged EC particles.*

The reviewer made a very good point here. As discussed in the manuscript, the apparent HGF may underestimate the hygroscopicity of BC particles when particles are not spherical shape. We attribute this the major reason of the difference between κ_{CCN} and κ_{HTDMA} in the beginning of experiment. However, due to the fast growth of BC particles in our study, the morphology of BC particles shifted from fractal to spherical shape within a very short time. Therefore, the apparent HGF at the end of experiments can represent real HGF of particles.

Besides, in the CCN data processing, the particle mass equivalent diameter was used as the particle dry diameter in the calculation of κ_{CCN} value by Equ (10). Therefore, the κ_{CCN} should reflect the real hygroscopicity of BC particles from this point of view.

(3) *What was the final size of the new particles from nucleation in the chamber? It could be a concern if the nucleation in the chamber was fast and the new particles grew too fast into the size range of the aged soot particles and hence interfere with the property measurements.*

Nucleation occurred in the chamber during several experiments of this study. Moreover, the newly formed particles grew along with BC particles inside the chamber. However, as shown in the Figure below, the difference in the peak diameter between BC particles and nucleation particles was always larger than 80 nm for all experiments. Therefore, the influence of nucleation particles to the measurement of BC properties was insignificant.

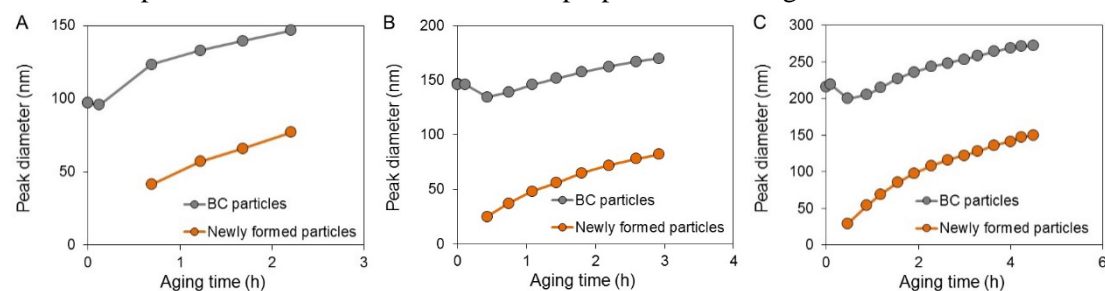


Figure 1. Peak diameter of BC and nucleation particles inside the chamber during experiments with initial BC diameter of 100 nm (A), 150 nm (B), and 200 nm, respectively.

1 **Aging and hygroscopicity variation of black carbon particles in Beijing**

2 **measured by a quasi-atmospheric aerosol evolution study (QUALITY) chamber**

3 Jianfei Peng^{1, 2*}, Min Hu^{1, 3*}, Song Guo^{1, 2}, Zhuofei Du¹, Dongjie Shang¹, Jing Zheng¹, Jun
4 Zheng², Limin Zeng¹, Min Shao¹, Yusheng Wu¹, Don Collins², Renyi Zhang^{1, 2*}

5 ¹State Key Joint Laboratory of Environmental Simulation and Pollution Control, College of
6 Environmental Sciences and Engineering, Peking University, Beijing, China 100871

7 ²Department of Atmospheric Sciences, Texas A&M University, College Station, Texas, USA
8 77843

9 ³Beijing Innovation Center for Engineering Sciences and Advanced Technology, Peking
10 University, Beijing, China 100871

11 *To whom correspondence should be addressed. E-mail: pengjianfeipku@gmail.com (Jianfei
12 Peng); minhu@pku.edu.cn (Min Hu); renyi-zhang@geos.tamu.edu (Renyi Zhang)

13 **Abstract.** Measurements of aging and hygroscopicity variation of black carbon (BC) particles
14 in Beijing were conducted using a 1.2 m³ quasi-atmospheric aerosol evolution study
15 (QUALITY) chamber, which consisted of a bottom flow chamber where ambient air was pulled
16 through continuously and an upper reaction chamber where aging of BC particles occurred.
17 Within the reaction chamber, transmission of the solar ultraviolet irradiation was approximately
18 50% - 60%, wall loss of primary gaseous pollutants was negligible compared with the replenish
19 rate by gas exchange, and BC exhibited a half-lifetime about 3-7 hours. Typically, equilibrium
20 for the primary gases, temperature, and relative humidity between the reaction chamber and
21 ambient air was established within 1 hour. Rapid growth of BC particles was observed, with
22 an average total growth of 77±33nm and average growth rate of 26±11 nm h⁻¹. Secondary
23 organic ~~aerosol~~aerosols (SOA) accounted for more than 90% of the coating mass. The O/C
24 ratio of SOA was 0.5, lower than the ambient level. The hygroscopic growth factor of BC
25 particles decreased slightly with an initial thin coating layer because of BC reconstruction, but
26 subsequently increased to 1.06-1.08 upon further aging. The κ (kappa) values for BC particles
27 and coating materials were calculated as 0.035 and 0.040 at the subsaturation and
28 supersaturation conditions, respectively, indicating low hygroscopicity of coated SOA on BC
29 particles. Hence, our results indicate that initial photochemical aging of BC particles does not
30 appreciably alter the particle hygroscopicity in Beijing.

31

32 1 Introduction

33 Atmospheric aerosols undergo continuous and complicated transformation during their
34 residence time in the atmosphere. The aging of aerosols is likely resulted from both physical
35 (i.e., coagulation, condensation, equilibrium partitioning, and evaporation) and chemical (i.e.,
36 photochemical gas-phase oxidation and multi-phase reactions) processes (Zhao et al., 2006;
37 Qiu et al., 2013; Zhang et al., 2015). Also, there are typically large variations in the particle
38 properties (i.e., size, mass, chemical composition, morphology, and optical and hygroscopic
39 parameters) during aging, significantly influencing the aerosol impacts on visibility, human
40 health, weather, and climate (Jacobson, 2001; Guo et al., 2014). A better understanding of the
41 aging process of aerosols in the atmosphere is critical in atmospheric and climate research.

42 For example, the scientific interest in the climate effects of black carbon (BC) has
43 remained, since BC is the strongest absorber of visible solar radiation (Wang et al., 2013). BC
44 solar absorption represents a central issue in climate change research, since the synthesis of
45 satellite, in situ, and ground observations shows that the global solar absorption (direct
46 radiative forcing or DRF) by BC is as much as $0.9 \text{ W} \cdot \text{m}^{-2}$, second only to that of CO_2 (Jacobson,
47 2001; Bond et al., 2013; IPCC, 2013). BC also represents an important component of air
48 pollution for large parts of the world (Zhang et al., 2015). The properties of BC are considerably
49 modified during aging, including the size, mass, morphology, and optical and hygroscopic
50 parameters (Khalizov et al., 2009; Xue et al., 2009a). Enhanced light absorption of BC particles
51 during aging not only contributes to atmospheric stabilization and exacerbation of haze
52 formation, but also imposes large positive radiative forcing on climate (Peng et al., 2016).
53 Furthermore, the variation in hygroscopicity during aging also regulates the lifetimes of BC
54 particles. Hygroscopic particles serve efficiently as cloud condensed nuclei (CCN), affecting
55 the formation, longevity and albedo of clouds (Yuan et al., 2008; Wang et al., 2011). Also,
56 deposition of BC particles, via in-cloud scavenging and wet deposition, depends highly on the
57 particle hygroscopicity (Bond et al., 2013). In addition, the hygroscopicity also affects the
58 aqueous-phase reactions of atmospheric pollutants (Ervens et al., 2011; Wang et al., 2016).
59 Previous studies using hygroscopic tandem differential mobility analyzer (H-TDMA)
60 instruments have shown that coating of hydrophilic materials significantly increases the
61 hygroscopic growth factor of BC particles (Saathoff et al., 2003; Khalizov et al., 2009; Guo et
62 al., 2016). The ability of BC particles to form CCN also enhanced after coating of hydrophilic
63 materials (Kuwata et al., 2007; Tritscher et al., 2011; Ma et al., 2013; Wittbom et al., 2014).
64 The activation supersaturation depends on the particle size, hygroscopicity of coating materials,
65 and the coating thickness (Ma et al., 2013). The coating materials in the previous experiments
66 include sulfuric acid (Zhang and Zhang, 2005; Khalizov et al., 2009), oxidation products from
67 biogenic and anthropogenic hydrocarbon species (Saathoff et al., 2003; Ma et al., 2013;
68 Khalizov et al., 2013), or secondary organic aerosols (SOA) from single emission source
69 (Tritscher et al., 2011). However, there still exist uncertainties for parametrization of the BC
70 lifetime in atmospheric models, because of insufficient constraints on the hydrophobic to
71 hydrophilic conversion of BC particles under variable ambient conditions.

72 Atmospheric field measurements have been performed to evaluate aging of particles on
73 different platforms, e.g., ground, aircraft, and cruise (Moffet and Prather, 2009; DeCarlo et al.,
74 2010; Peng et al., 2014; Liu et al., 2015) and over different spatial scales (intensive campaigns

75 or long-term measurements). Typically, a wide variety of state-of art instruments are employed
76 to characterize the changes of the chemical and physical properties of aerosols. On the other
77 hand, field measurements at fixed sites are affected by transport, local emissions, and chemistry,
78 and quantification of the particle parameters during aging involves complex decoupling of the
79 various processes (Peng et al., 2016). In particular, it is challenging to isolate the chemical
80 processes from those related to meteorology (i.e., transport and mixing) and emissions.

81 The methods of environmental chambers or reactors have been widely employed in
82 atmospheric chemistry research, including photochemical oxidation of volatile organic
83 compounds (VOCs) (Zhang et al., 2000), formation and growth of aerosols (Claeys, 2004;
84 Kalberer, 2004), nucleation of nanoparticles (Zhang et al., 2004; Wang et al., 2010; Zhang et
85 al., 2012), aging of BC particles (Zhang et al., 2008), and cloud formation (Ruehl et al., 2016).
86 Dependent of the scientific objectives, the designs of environmental chambers and reactors
87 vary considerably (Zhang et al., 2015). However, few of the previous experimental methods
88 ~~are able to characterize~~ have characterized the evolution of aerosols under the ambient
89 conditions.

90 In this study, we present measurements of aging and hygroscopicity variation of BC
91 particles in Beijing using a quasi-atmospheric aerosol evolution study (QUALITY) chamber
92 (Reed, 2010; Peng et al., 2016). The performance of the QUALITY chamber for mimicking
93 the ambient gaseous concentrations (i.e., the wall loss, and gas mixing rate), ultraviolet
94 transmission, and meteorology parameters (i.e., temperature and relative humidity, RH) has
95 been evaluated.

96 2 Experimental method

97 The 1.2 m³ QUALITY chamber was employed to study BC aging under ambient
98 conditions (Fig. 1). The two-layer chamber was comprised of an inner layer of 0.13 mm
99 ~~polytetrafluoro-ethylene~~ Perfluoroalkoxy alkane (PFA) Teflon and an outer rigid 5.6 mm thick
100 acrylic shell (Cyrus Industries Acrylite, OP-4). Both Acrylite OP-4 Acrylic and PFA Teflon
101 allowed for efficient ultraviolet (UV) transmission in UV-B (280-315 nm) and UV-A (315-400
102 nm) ranges. When exposed to sunlight, the UV light transmitted through the chamber wall and
103 initiated photochemical reactions inside the chamber.

104 The two individual subdivisions of the QUALITY chamber included a bottom flow
105 chamber, where ambient air was pulled through continuously over each experiment, and an
106 upper reaction chamber, where aging of BC particles occurred (Fig. 1). The two chambers were
107 separated by a 5 μm thick semi-permeable expanded polytetrafluoroethylene (e-PTFE)
108 membrane with high degrees of chemical resistivity, microporosity, nonpolarity, and thermal
109 stability. Gaseous species penetrated the membrane by either bulk gas flow or diffusion. The
110 permeability of the e-PTFE was greater than 90 % for nearly all the tested volatile organic
111 components (Fig. S1) and other gaseous pollutants, i.e., SO₂, NO_x, O₃ and CO. Particles, on
112 the other hand, were blocked from penetration into the reaction chamber. The filtration
113 efficiency of the e-PTFE membrane was measured to be over 99.5% for particles larger than
114 15 nm. During each chamber experiment, ambient air was pulled through the flow chamber
115 continuously and gases in lower chamber permeated through the membrane into the reaction
116 chamber. Hence, an environment that continuously captured the ambient gas concentrations

117 without the presence of ambient particles was created inside the reaction chamber. Since the
118 chamber was continuously exposed to ambient gas concentrations during experiments, gases
119 lost due to reaction, deposition or adsorption to the seed aerosols within the reaction chamber
120 were steadily replenished by the exchange with the flow chamber. Several sampling ports were
121 set at the side of the reaction chamber for injection of seed particles or sampling during
122 experiment.

123 Seed particles were introduced in the reaction chamber via an injection line (Fig. S2). To
124 investigate the growth of BC particles under ambient condition, monodisperse BC particles
125 were injected into the QUALITY chamber. BC particles were generated by incomplete
126 combustion of propane fuel in a custom-made laminar diffusion burner (Santoro et al., 1983;
127 Qiu et al., 2012). The aerosol stream sequentially passed through a 300°C heater to evaporate
128 the semi-volatile organic compounds in the particle phase, a Nafion dryer to remove excess
129 moisture in the flow, and four one-meter-long ~~eylindercylinders~~ containing both alumina
130 spherules coated with potassium permanganate and activated carbon to remove all the
131 gaseous pollutants (i.e., VOCs, H₂S, SO₂, NO_x, O₃). The combined measurement of particle
132 size distribution, density and chemical composition exhibited that organics accounted for less
133 than 10% of fresh BC mass concentration. Moreover, the single scattering albedo (SSA) of
134 fresh BC particles was only 0.1, further confirming that few organic coatings existed on fresh
135 BC particles after treatment. The measured removal efficiency in the cylinders for SO₂, NO
136 and NO₂ were 99.2%, 100%, and 99.9%, respectively. The aerosol stream was then introduced
137 through an ionizer and into a differential mobility analyzer (DMA, model 3081, TSI, Inc.) with
138 stable voltage to create a monodisperse BC particles flow.

139 A suite of high time resolution state-of-the-art aerosol instruments simultaneously
140 measured a comprehensive set of BC properties throughout the BC aging process- (Table S1).
141 The particle diameter, mass, chemical composition, hygroscopicity and ability as cloud
142 condensation nuclei (CCN) were measurement by a scanning mobility particle sizer (SMPS),
143 a differential mobility analyzer–aerosol particle mass analyzer (DMA-APM) system, a high-
144 resolution time-of-flight aerosol mass spectrometer (HR-ToF-AMS), a humidified tandem
145 differential mobility analyzer (HTDMA) system, and a cloud condensation nuclei counter
146 (CCNC), respectively. Detail information of the instruments is provided in the supplementary
147 material and previous publications (DeCarlo et al., 2006; Khalizov et al., 2009). Specific
148 measurement procedures in this study are discussed below.

149 **DMA-APM measurement.** The DMA-APM was used to measure the effective density of BC
150 particles (Pagels et al., 2009). Before any DMA-APM measurement, a SMPS scan was made
151 to obtain the size distribution of particles inside the chamber. The particle size distribution was
152 then fitted with a lognormal Gaussian distribution to derive the peak diameter. During a DMA-
153 APM measurement, the aerosol flow passed through DMA with a fixed voltage to select
154 particles with a fixed diameter. The APM then measured the mass distribution of the selected
155 particles with the same diameter, and the effective density of these particles was obtained by
156 fitting the mass distribution with a normal Gaussian distribution.

157 **DMA-CCN measurement.** Similar to the density measurements, CCN activation was also
158 measured on the basis of monodisperse particles with a peak diameter. A DMA with a fixed

159 voltage selected particles with a peak diameter. Both a CPC and a CCN counter were placed in
160 parallel after the DMA to simultaneously measure the total particle number concentration (N_{cn})
161 as well as the activated number concentration (N_{ccn}) at a fixed supersaturation. The activation
162 fraction of the BC particles with peak diameter is calculated as:

$$163 \quad f_{CCN} = \frac{N_{CN}}{N_{CCN}} \quad (1)$$

164 Several gradients of supersaturation were set for the CCN counter, with each one being 6
165 min. This method yielded a steeper curve of the CCN activation rate, which was employed to
166 estimate the particle diameter with 50% activation fraction (D_{50}) and the kappa value.

167 Prior to each experiment, the QUALITY chamber was flushed by zero air for more than
168 40 hours to ensure a clean condition and covered with two layers of anti-UV cloth to shield it
169 from sunlight. In the beginning of each experiment, monodisperse BC particles were
170 introduced into the chamber. The injection of BC particles typically lasted for 1 to 2 hours.
171 During the injection period, zero air passed through the bottom chamber continually to remove
172 any possible remaining gaseous pollutant that were removed by the activated carbon. After the
173 injection, ambient air was pulled through the bottom chamber at a flow rate of about 50 L min^{-1}
174 for at least half an hour in order to produce a quasi-ambient condition inside the chamber.
175 Finally, the anti-UV cloth was removed, and BC particles underwent aging inside the reaction
176 chamber. A charged zero air stream continuously passed through the space between the two
177 chamber layers to reduce particle wall loss. Various properties of BC particles, including the
178 particle diameter, mass, chemical composition, hygroscopicity, and optical coefficients, were
179 simultaneously measured by a suite of state-of-art aerosol instruments in every 0.5 - 1 hour.
180 Ambient particles and chamber particles were measured alternately every 30 min. The aging
181 experiments lasted for about 2-6 hours depending on the initial BC concentrations and ambient
182 conditions.

183 The BC aging experiments were conducted from August 18th to October 17th, 2013 at an
184 urban site ([PKUERS](#)) located on the campus of Peking University in the northwestern Beijing
185 (39.99°N , 116.31°E) (Hu et al., 2012).

186 **3. Characterization and Validation of the QUALITY chamber**

187 **3.1 Wall loss of gases and aerosols**

188 To evaluate the wall loss of both particles and gases in the QUALITY chamber, different
189 gaseous pollutants and particles were introduced into the chamber separately and the decay of
190 their concentration inside the chamber was measured by gas analyzers and SMPS, respectively.
191 All of the ports connected to the ambient air were closed to ensure an enclosed system in the
192 reaction chamber.

193 Particles with different chemical composition exhibited different wall loss rates.
194 Monodispersed BC particles with different diameters showed a small half-lifetime (τ) of about
195 4-7 hours (Reed, 2010). Aerosol nucleation also occurred inside the chamber likely from
196 organic species (Zhao et al., 2009), which corresponded to a half time of about 3.5 hours (Fig.
197 S3), because the nucleated particles inside the chamber was neutral with a slow electrostatic

198 loss to the wall.

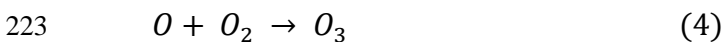
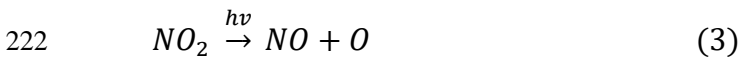
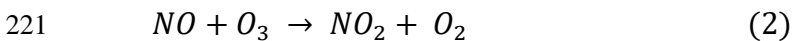
199 Gas species had a longer residence time inside the chamber. Toluene and isoprene did not
200 show obvious wall loss during a two-day experiment (Reed, 2010). O₃, SO₂ and NO_x decreased
201 by 50% inside the chamber after more than 20 hours, suggesting slow loss. Since the loss rate
202 of these primary gaseous pollutants was much slower than the gas exchange rate between the
203 chamber, the loss of gases was replenished by the exchange with the flow chamber.

204 3.2 UV transmission

205 The QUALITY chamber contained two layers of walls, an acrylic shell layer and a PFA
206 Teflon layer. Since the QUALITY chamber used sunlight as the photochemical origin, the
207 transmission spectra of the two-layer walls was of great important for the photochemical
208 reactions inside the reaction chamber.

209 The transmission efficiencies of each material were measured using ~~a Fourier transform~~
210 ~~infrared spectroscopy (FTIR) system~~ an ultraviolet-visible (UV-Vis) spectrophotometry
211 (PerkinElmer Inc., model 552). As shown in Figure 2, the Teflon film exhibited stable
212 transmission efficiency of about 60% in the focused wavelength range. The Acrylic shell,
213 however, showed very low transmission efficiency when the wavelength range was shorter
214 than 270 nm, and high transmission efficiency (nearly 90%) when the wavelength range was
215 longer than 300 nm. In general, approximately 60% of the UVA irradiation (315-400 nm range)
216 and 50% of the UVB irradiation (280-315 nm range) penetrated through the chamber walls,
217 allowing photochemical processes to take place in the upper reaction chamber.

218 A NO₂-photolysis experiment was also conducted to characterize the UV transmission of
219 QUALITY chamber. NO₂ was introduced inside the chamber at a clean and sunny day.
220 Reactions among NO₂, NO and O₃ will occur as the following equations:



224 By simultaneously monitoring the concentrations of NO₂, NO and O₃ inside the chamber,
225 the photolysis constant of NO₂, J(NO₂), inside the chamber was estimated. The photolysis
226 constant of NO₂ inside the chamber was on average 55% of that in the ambient air, in agreement
227 with the transmission spectra measurement, further confirming that the two-layer chamber
228 walls allowed 50% - 60% of solar irradiation in the UV range into the reaction chamber.

229 3.3 ~~Exchange of gases between~~ Gas concentrations in the reaction chamber

230 To investigate the VOCs concentration inside the reaction chamber after the injection of
231 BC particles, both the chamber and ambient air was sampled with VOC canisters just before
232 the BC aging experiment started. These canisters were then analyzed by a gas chromatography-
233 mass spectrometer / flame ionization detector (GC-MS/FID, HP inc.) system (Liu et al., 2008).
234 The concentrations of VOCs containing 4 or more carbons are illustrated in Figure 3. Slightly
235 higher concentrations of several VOCs in the QUALITY chamber, e.g., n-butane, n-pentane,

236 toluene, were observed compared with those in the ambient air, due to the co-injection of a
237 small amount of VOCs together with BC particles into the chamber. Nevertheless, the average
238 increase of the VOC concentrations was only 16% or 0.1 ppb for all focused VOCs species,
239 with the largest increase of 35% or 0.36 ppb, suggesting the insignificant influence of soot
240 burner on VOCs concentrations and SOA formation in the chamber.

241 Additional experiments were conducted to characterize the exchange time scale for gases
242 in the QUALITY chamber. The chamber was firstly cleaned and flushed with zero air for 40
243 hours. Ambient air was then pulled through the bottom chamber (Fig. 34), and the
244 concentrations of gaseous pollutants, including O₃, NO_x, CO, and SO₂, were measured
245 alternatively in the ambient air and in the upper chamber. In the beginning of the experiment
246 the concentrations of all gaseous species were lower than those in the ambient air. After ambient
247 air was pulled through the bottom chamber (labeled as the black dots in Fig. 34), the
248 concentrations of the gaseous pollutants in the reaction chamber increased sharply. For
249 example, the CO concentration inside the chamber was approximate 70% of that the ambient
250 concentration after 30-min mixing. The concentrations inside the chamber and ambient air
251 exhibited little difference after 1-hour mixing (Fig. 3e4c). Hence, the QUALITY chamber well
252 replicated the ambient gas concentrations. The gas exchange rate between the bottom and
253 reaction chambers was calculated to be approximately 0.06 min⁻¹.

254 3.4 Temperature and RH

255 The greenhouse effect for an outdoor chamber typically increases the temperature and
256 decreases the RH inside the chamber. For the QUALITY chamber, however, heat produced by
257 the greenhouse effect inside the chamber was effectively taken away as the ambient air
258 continuously passed through the bottom chamber and exchanged with air in the upper chamber.
259 As illustrated in Figure 45, there was little difference in temperature or RH inside and outside
260 the chamber, when the chamber experiments lasted for more than 1 hour, suggesting that the
261 QUALITY chamber effectively captured the ambient temperature and RH.

262 3.5 Sulfuric acid production

263 Though gaseous pollutants such as SO₂, O₃, NO_x and VOCs penetrated into the reaction
264 chamber from the bottom chamber through the semi-permeable membrane, low volatile and
265 sticky gases, i.e., sulfuric acid, were unlikely to penetrate through the membrane (Fortner et al.,
266 2004). To characterize sulfuric acid production inside the chamber, we conducted a special
267 experiment by pulling ambient air into the bottom chamber, while injecting SO₂ directly into
268 the reaction chamber. The experiment was conducted around noon on a clean day when the O₃
269 concentration was around 50 ppb. A custom-made atmospheric pressure-ion drift chemical
270 ionization mass spectrometry (AP-ID-CIMS) (Fortner et al., 2004; Zheng et al., 2010) was used
271 to directly measure the concentration of gaseous sulfuric acid. Fig. 56 shows a good correlation
272 between SO₂ and gaseous H₂SO₄ inside the chamber, suggesting that the QUALITY chamber
273 well simulated the formation of low volatile gaseous species and hence the photochemical
274 processes.

275 4. BC evolution in the QUALITY chamber

276 Time series of the ambient PM, gas, and meteorology parameters of ambient air during

chamber experiment period are illustrated in Figure 67. Except for the last experiment conducted on October 17th, all experiments were conducted between August 18th, 2013 and September 21st, 2013. During this period in Beijing, strong photochemical reactions and frequent heavy pollution events occurred (Huang et al., 2010; Zhao et al., 2013). Temperature and RH during this period (August 18th to September 21st) varied from 24°C to 38°C and from 20 % to 90 %, respectively. The average concentration of PM_{2.5}, SO₂ and NO_x were 60 ± 45 μg m⁻³, 3.2 ± 2.6 ppb and 33.9 ± 20.9 ppb, respectively.

The red shaded areas in Figure 67 represent the period of the nine chamber experiments. In general, chamber experiments were conducted in the afternoon of relatively clean and sunny days, when strong solar radiation led to fast photochemical reactions. There were two experiments conducted under polluted days, e.g., the experiments on October 22nd and September 11th. Table 1 summaries the conditions of the experiments. Totally, 10 BC aging experiments were conducted, including four experiments using BC particles with initial mobility diameter of 100 nm, three experiments using 150 nm particles, and three using 220 nm BC particles. The average concentrations of PM_{2.5} and NO_x over each chamber experiment were only 9 to 69 μg m⁻³ and 9 to 41 ppb, respectively. The concentrations of VOCs, such as toluene and m/p-xylene were relatively low during most of the experiments compared with severe pollution episodes in Beijing (Guo et al., 2014). *J*(O¹D) and O₃ exhibited higher values during the chamber experiments. The average *J*(O¹D) values and O₃ concentrations ranged from 3.2 × 10⁻⁶ s⁻¹ to 21.1 × 10⁻⁶ s⁻¹ and 26 to 92 ppb, respectively.

4.1 BC growth

To quantify the growth of BC particles, several parameters were used to describe the properties of BC particle, including the effective density, mobility diameter and mass equivalent diameter. Material density (ρ_m) is the average density of the solid and liquid material in the particle. Assuming that the volume of the species coexisting in an individual particle does not change upon mixing, the density of an internally mixed particle is calculated using the material densities and mass concentrations of particulate constituents (DeCarlo et al., 2004; Pagels et al., 2009),

$$\rho_m = \frac{\sum_{species} m_i}{\sum_{species} V_i} = \frac{\sum_{species} m_i}{\sum_{species} \frac{m_i}{\rho_i}} = \frac{\sum_{species} MC_i}{\sum_{species} \frac{MC_i}{\rho_i}} \quad (5)$$

where ρ_i is the material density of species *i*, V_i is its volume, m_i is its mass, and MC_i is its mass concentration. This approach is based on the assumption that there is no void space enclosed within the particle envelope. Hence, the material density is larger than the true particle density with internal voids in particles. In this study, ρ_m is calculated from the chemical composition of coating materials measured by AMS. A value of 1.35 for the material density of SOA formed during chamber experiment was obtained by directly measuring the density of newly form particles inside the chamber via DMA-APM system.

Effective density (ρ_{eff}) is defined as the ratio of the measured particle mass (m_p) to the particle volume calculated assuming a spherical particle with a diameter equal to the measured

316 mobility diameter (D_m) (DeCarlo et al., 2004; Pagels et al., 2009; Xue et al., 2009b):

$$317 \quad \rho_{eff} = \frac{6m_p}{\pi D_m^3} \quad (6)$$

318

319 In this study, m_p of BC particles was measured by the APM and mobility diameter (D_m)
320 was measured by the DMA. The effective density reflects the information on both particle
321 density and shape. If particles are spherical in the absence of internal void, the effective density
322 equals the material density. If particles are non-spherical, the calculated volume and volume
323 concentration are larger than the true values, and the effective density is less than true particle
324 and the material density.

325 Figure 78 exhibits the change of particle density and diameter in three typical BC aging
326 experiments using BC particles with the initial diameter of 100 nm, 150 nm, and 220 nm
327 (experiment #4, #5, and # 9 in Table 1, respectively). The average $PM_{2.5}$
328 ~~concentration~~ concentrations in these experiments ~~was~~were 40, 27, and 12 $\mu\text{g m}^{-3}$, respectively,
329 suggesting relatively clean conditions during the experiments. In all three experiments, aging
330 of BC particles occurred between 13:00-14:00 and 17:00 in the afternoon. The highest $J(O^1D)$
331 value varied from 1.7 to $2.4 \times 10^{-5} \text{ s}^{-1}$ and decreased generally over the experiment period.
332 Average O_3 concentrations during the three experiments were 68, 83 and 54 ppb, respectively,
333 indicating strong oxidation during the experiment periods.

334 ~~The~~For three initial ρ_{eff} values of BC particles were 0.46, 0.34 and 0.25 g cm^{-3} for particles
335 ~~with the initial diameter~~ D_m of 100 nm, 150 nm, and 220 nm, the ranges of effective density of
336 fresh BC particles in each experiment were 0.43-0.50 g cm^{-3} , 0.34-0.34 g cm^{-3} , and 0.24-0.32
337 g cm^{-3} , respectively, indicating highly fractal BC aggregates ~~with chain-like branches~~ (Zhang
338 et al., 2008). The small variation for particles with the same D_m also demonstrated the
339 consistency of fresh BC morphology in different experiments. After aging of 1 hour, ρ_{eff} of BC
340 particles in the three experiments increased to approximately 1.2 g cm^{-3} , suggesting that
341 formation of the secondary components changed the morphology from chain-like BC particles
342 into a more compact shape (Zhang et al., 2008; Peng et al., 2016). The morphology change was
343 further confirmed by a decrease of D_m , particularly for larger BC particles that were more
344 fractal than smaller BC particles.

345 As the D_m is largely influenced by the particle morphology, we utilized the parameter of
346 mass equivalent diameter (D_{me}) to describe the growth of particles. Based on the mobility
347 diameter (D_m), material density (ρ_m) and effective density (ρ_{eff}), the D_{me} is calculated assuming
348 that particles are compact and with a spherical morphology (DeCarlo et al., 2004):

$$349 \quad D_{me} = \sqrt[3]{\frac{\rho_{eff}}{\rho_m}} D_m \quad (7)$$

350

351 The change in the mass equivalent diameter (ΔD_{me}) during BC aging is defined as the total
352 coating thickness, and the ratio of the total coating thickness to the initial mass equivalent

353 diameter ($\Delta D_{me}/D_{me,0}$) is defined as the coating fraction.

354 The initial D_{me} of fresh BC particles with initial D_m of 100, 150 and 220 nm were 61, 84
355 and 114 nm, respectively. In contrast to the mobility diameter, D_{me} increased continuously
356 during the entire experiment. After 3-4 hours, D_{me} in the three experiments increased to 133,
357 169 and 197 nm, respectively (Fig. 78), with the average growth rates of 19, 29 and 31 nm h⁻¹.
358 Higher growth rates in D_{me} occurred around noontime, when the $J(O^1D)$ value was higher and
359 the photochemical reaction was stronger. On the other hand, much less growth rate was
360 observed during late afternoon or with cloud coverage (As shown in Fig. 7e8c at 15:00),
361 indicating that the growth was driven by photochemical reactions.

362 The increases of the particle density and diameter in all the experiments are summarized
363 in Table 2. Fast aging of BC particles occurred in all experiments. The total growth of D_{me}
364 ranged from 40 nm to 152 nm within 3-6 hours, with an average growth of 73 nm. The average
365 growth rate was 26 ± 11 nm h⁻¹, demonstrating large secondary production under the ambient
366 conditions in Beijing. The largest growth rate ($\Delta D_{me} = 152$ nm) was observed in experiment
367 #8, when solar irradiation was the strongest among all experiments (Table 2).

368 Correlation analysis was made between the average growth rate of BC particles ($\Delta D_{me}/\Delta t$)
369 with O_3 , $PM_{2.5}$, $J(O^1D)$, and temperature during the different experiments (Fig. S4). The growth
370 rate of BC particles exhibits no correlation with O_3 concentration ($R^2=0.00$), weak negative
371 correlation with $PM_{2.5}$ concentration ($R^2 = 0.25$), and strong positive correlations with $J(O^1D)$
372 ($R^2 = 0.80$) and temperature ($R^2 = 0.67$), indicating the importance of photochemical production
373 on the BC coating materials.

374 4.2 Chemical composition of coating materials

375 Particle composition measurements by AMS during chamber experiments reveal a
376 majority of coating materials (above 90%) as SOA (Fig. 78). The concentration of SOA inside
377 the chamber reached up to $9 \mu\text{g m}^{-3}$ in several experiments, suggesting fast formation of SOA
378 via gas phase oxidation of VOCs. The SOA formation in Beijing is likely attributed to a large
379 amount of anthropogenic aromatic VOCs (Peng et al., 2017).

380 The elemental compositions of OA inside the chamber, i.e., the oxygen to carbon (O/C)
381 ratio and the hydrogen to carbon (H/C) ratio, were calculated based on the updated ambient
382 calibrations (He et al., 2011; Canagaratna et al., 2015). The H/C and O/C ratios of organics for
383 coating on BC particles exhibit notable trends during the aging process. Figure 8A9A shows
384 an example of the evolution of H/C and O/C ratios in experiment #8. The data were corrected
385 for the CO_2 concentration in the chamber, which were introduced into the chamber with BC
386 particles and influenced the abundance of $m/z = 28$ and 44 in the AMS mass spectra. The H/C
387 ratio decreased from 1.73 to 1.45 over six hours. Accordingly, the O/C ratio increased from
388 0.32 to 0.50 during the same time, revealing that further oxidation of SOA occurred in the latter
389 part of the experiment. The lower final O/C ratio (0.5) in the chamber experiment (0.5) than
390 that under the ambient conditions (Hu et al., 2016) implies that there are oxidation on a longer
391 timescale or by the aqueous pathway for the formation of highly oxidized SOA in the ambient
392 air (Zhang et al., 2015).

393 Furthermore, the mass spectra of OA inside the chamber shows strong correlation with the

394 less-oxidized oxygenated organic aerosols (LO-OOA) derived from field measurements in
395 Beijing (Hu et al., 2016), which likely arose from oxidation of aromatic VOCs emitted from
396 vehicles (Peng et al., 2017). The correlation coefficient (R^2) initially was 0.88 and raised to 0.99
397 sharply (Fig. 8B9B), indicating that the chamber well simulated the formation of LO-OOA.

398 In our study, the secondary inorganic aerosols, i.e., sulfate, nitrate and ammonium, only
399 accounted for less than 10% of the coating materials on BC particles. This is consistent with
400 the previous studies showing that the concentration of organics is much larger than those of
401 sulfate and nitrate during the early stage of haze development in Beijing (Guo et al., 2014).
402 The low observed sulfate concentration in this study suggests that the gas phase formation of
403 sulfuric acid was unimportant under our experimental conditions. On the other hand, it has
404 been shown that the aqueous-phase reactions represent the dominate pathway for sulfate
405 formation in Beijing (Guo et al., 2010; Wang et al., 2016).

406 NO_2 has a higher reaction coefficient with the OH radical ($8 \times 10^{-12} \text{ cm}^3 \text{ molecule}^{-1} \text{ s}^{-1}$)
407 than SO_2 (Zhang et al., 2015). Nitrate acid formed in the gas phase is transformed into nitrate
408 salts by the reaction with ammonia in the equilibrium process:



410 The equilibrium of this reaction is highly depended on ambient temperature and RH (Zheng et
411 al., 2008). In this study, chamber experiments were conducted in the afternoon with high
412 temperature and low RH (Table 1), which shifted the thermodynamic equilibrium to the gas
413 phase.

414 4.3 Hygroscopicity evolution

415 HTDMA measurement

416 The hygroscopic growth factors (HGF) of particles in each experiment were continuously
417 measured by the HTDMA system and corrected for the reference “dry” diameters,

$$418 \quad \text{HGF} = \frac{D_{wet,t}/D_{m,t}}{D_{dry,0}/D_{m,0}} \quad (9)$$

419 where D_m is the mobility diameter of fresh or coated particles at dry condition, D_{dry} is the
420 mobility diameter of particles after experiencing a low humidity (below 30%) cycle in
421 HTDMA, and D_{wet} is the mobility diameter of particles after experiencing a high humidity
422 cycle (87%) in HTDMA.

423 Figure 910 shows the hygroscopicity variation of BC particles with the initial mobility
424 diameter ($D_{m,0}$) of 100 nm and 150 nm. The measured HGF of 0.999 - 1.004 for fresh BC
425 particles suggests high hydrophobicity, consistent with the previous studies (Khalizov et al.,
426 2009; Weingartner et al., 1997). After exposed to sunlight and ambient gaseous pollutants for
427 several hours, the HGF of these BC particles increased to 1.02-1.08 at the end of each
428 experiment. The HGF value varied with the total growth (ΔD_{me}) of BC particles, but was
429 constant at the same ΔD_{me} for different experiments (Fig. 910). The final HGF values shown
430 in Figure 910 (1.02-1.08) were much lower than those in previous laboratory studies (Khalizov

431 et al., 2009; Tritscher et al., 2011) but similar to the low hygroscopic fraction in field
432 observations (Swietlicki et al., 2008), even for growth of particle size up to 90 nm in our
433 experiments.

434 The HGF is affected by many factors, e.g., the particle chemical composition and
435 morphology as well as RH (Qiu et al., 2012). The hygroscopicity of BC particles coated with
436 inorganic components, i.e., sulfuric acid (Khalizov et al., 2009), is significantly higher than
437 that coated by organic compounds (Tritscher et al., 2011). In this study, the major component
438 of the coating substance was LO-OOA with a O/C ratio about 0.5. The low oxygen content of
439 SOA coated on BC particles explains the low hygroscopicity (Jimenez et al., 2009), indicating
440 that coating of BC particles during the early stage haze development in Beijing does not
441 considerably increase the particle hygroscopicity.

442 The morphology of BC particles directly affects the HGF. As illustrated in Figure 1011,
443 when the ΔD_{me} was 18 nm and 22 nm for 100 nm and 150 nm BC particles, respectively, the
444 HGF decreased slightly to about 0.99, suggesting that a thin layer of coatings on BC particles
445 decreased the particle diameter, even though a certain amount of water absorbed by BC
446 particles increased the particle mass. The surface tension of the water layer produced an inward
447 force on the “chain-like” branches of BC particles, leading to particle reconstruction, and a
448 more compact morphology. Such change was also identified in laboratory studies (Weingartner
449 et al., 1997; Tritscher et al., 2011; Qiu et al., 2012). In this study, the BC particles became
450 spherical when ΔD_{me} was 30 nm and 40 nm for particles with initial D_m of 100 nm and 150 nm,
451 respectively (Peng et al., 2016). Therefore, when ΔD_{me} was large, the HGF value was not
452 influenced by reconstruction.

453 CCN measurements and κ closure

454 The CCN activation fraction (f_{CCN}) of BC particles at different supersaturation during two
455 typical experiments is illustrated in Figure 1011. Fresh BC particles were not activated even at
456 very high supersaturation conditions (0.7%). With aging, f_{CCN} rapidly raised to nearly 100% at
457 high supersaturation (0.7% for experiment #4 and 0.6% for experiment #6). After several hours,
458 BC particles became CCN at lower supersaturation. The f_{CCN} at 0.4 supersaturation (Fig. 11a
459 in experiment #4) and 0.3 supersaturation (Fig. 11b in experiment #6) exceeded 50% before
460 the end of these two experiments, suggesting that aging increases the ability of BC particles to
461 become CCN (Wittbom et al., 2014) and a large amount of coatings results in activation at
462 lower supersaturation.

463 To further investigate the hygroscopicity of BC particles and combine the measurements
464 using HTDMA and CCN, we evaluated the hygroscopicity parameter, kappa (κ) (Petters and
465 Kreidenweis, 2007). The approximate relationship between the dry particle mass equivalent
466 diameter (D_{me}), the critical saturation ratio (S_c) and the apparent κ value of particles is describe
467 as:

$$468 \quad \kappa = \frac{4A^3}{27D_{me} \ln^2 S_c} \quad (10)$$

469 where A is a parameter that includes several features of the solvent,

$$A = \frac{4\sigma_{s/a}M_w}{RT\rho_w} \quad (11)$$

471 M_w is the molecular weight of water, ρ_w is the density of water, $\sigma_{s/a}$ is the surface tension of the
472 solution/air interface, R is the universal gas constant, and T is temperature.

473 In addition to the supersaturated condition, the κ theory also adopts the form for the
474 subsaturated condition, using the HGF from HTDMA measurement and RH:

$$\frac{RH}{\exp\left(\frac{A}{D_{wet}}\right)} = \frac{HGF^3 - 1}{HGF^3 - (1 - \kappa)} \quad (12)$$

476 where D_{wet} is the wet diameter of particles.

477 The apparent κ values of BC particles calculated by HTDMA (κ_{HTDMA}) and CCN
478 (κ_{CCN}) are shown in Figure 1011. The κ of fresh BC particles was near zero. With aging,
479 SOA coated on BC particles increased the κ_{HTDMA} and κ_{CCN} to approximately 0.04,
480 although the κ_{HTDMA} and κ_{CCN} exhibited difference features. A slightly higher κ_{CCN}
481 than κ_{HTDMA} at the beginning of aging was identified, attributed to reconstruction of BC
482 particles after humidified and underestimation of HGF and thus the κ_{HTDMA} value. Such a
483 difference between κ_{CCN} and κ_{HTDMA} was also observed in previous studies (Tritscher et
484 al., 2011; Martin et al., 2013). Nevertheless, the apparent κ values from two both methods were
485 comparable at the end of both experiments.

486

487 Assuming that a simple mixing rule is applicable to coated BC particles, the κ for coating
488 materials can be calculated based on the volume fraction of BC and SOA:

$$\kappa = \sum_i \varepsilon_i \kappa_i \quad (13)$$

490 where ε_i represents the volume fraction of species i . Since the SOA formed inside the
491 chamber was not highly hygroscopic, some of the SOA components might not be able to solve
492 in water droplets (Petters and Kreidenweis, 2008), leading to the underestimation of the κ
493 values of the coating materials in this study.

494 The κ values of the coating materials were 0.04 at the end of our experiments for both
495 CCN and HTDMA method, much lower than that of ambient aerosols in Beijing (Gunthe et al.,
496 2011; Wu et al., 2016) and those of SOA in previous chamber studies (Jimenez et al., 2009;
497 Tritscher et al., 2011; Martin et al., 2013). As discussed above, the coating substances on BC
498 particles were mainly SOA formed from photochemical oxidation. The κ of SOA depends on
499 the oxidation degree, which is correlated to the O/C ratio (Jimenez et al., 2009). ~~The O/C ratio~~
500 ~~of the coating SOA was 0.5 in our experiment, likely explaining the low κ with LO-OOA;~~
501 Massoli et al. 2010). The O/C ratio of the coating SOA was 0.5 in our experiment,
502 corresponding to the O/C ratio of approximately 0.4 in Jimenez et al. (2009) and Massoli et al.
503 (2010) duo the utilize of updated AMS calibration method in this study. The κ value of coating
504 materials here is in general slightly lower than those of SOA with similar oxidation degree
505 (O/C ratio) formed from different VOCs precursors (Jimenez et al., 2009; Massoli et al. 2010).

506 As motion above, the κ values of the coating materials might be underestimated duo to the
507 ignore of solubility of the SOA products. Also, our experiments represent the aging of BC
508 under typical urban condition, where variety of anthropogenic VOCs, i.e., toluene, xylene,
509 TMB and small molecular PAHs, contribute significantly to the SOA formation. Some products
510 of these VOC precursors may exhibit low hygroscopicity.

511 **5 Conclusions**

512 In this paper, we present measurements of aging and hygroscopicity of BC particles in
513 Beijing using the QUALITY chamber. The unique two sub-chamber design facilitates the
514 evaluation of aging of BC particles under ambient conditions, by mimicking the ambient
515 gaseous concentrations without the presence of ambient aerosols. High UV transmission
516 efficiency (50-60%) and negligible wall loss of primary gaseous pollutants are shown for the
517 chamber performance. The validation experiments demonstrate little differences in the primary
518 gas concentrations, temperature, and RH between the chamber and the atmosphere, suggesting
519 that the chamber captures the evolution of ambient conditions. In addition, our results show
520 sulfuric acid production correlated with SO₂, indicating that the chamber well simulates
521 photochemical-driven formation of low volatile gaseous species by the hydroxyl radical.

522 BC aging experiments were performed using the QUALITY chamber in Beijing. Fast
523 growth of BC particles (on average 26 ± 11 nm h⁻¹) was observed, and SOA was identified as
524 the dominate component of the coating materials on BC particles, while inorganic species, such
525 as sulfate and nitrate, were unimportant under our experimental condition and timescale.

526 The HGF of BC particles exhibited a very low value (1.02-1.08) after several hours aging.
527 A slight decrease of HGF with a thin coating layer indicated reconstruction of BC particles
528 after humidified. Also, a very low kappa value (0.035) for BC particles at both subsaturation
529 and supersaturation conditions were found, with HTDMA and CCN measurements. Hence, our
530 results indicate that initial photochemical aging of BC particles does not appreciably alter the
531 particle hygroscopicity in Beijing.—

532 **Acknowledgement**

534 This work was supported by National Natural Science Foundation of China (91544214,
535 41421064), the National Basic Research Program, China Ministry of Science and Technology
536 (Grant 2013CB228503, [Grant 2013CB955801](#)), National Natural Science Foundation of China
537 (Grant 21190052), and the China Ministry of Environmental Protection's Special Funds for
538 Scientific Research on Public Welfare (Grant 20130916). R.Z. acknowledged support from the
539 Robert A. Welch Foundation (Grant A-1417) and Houston Advanced Research Center. We
540 thanked Wei Hu and Zhaoheng Gong for their assistance with the AMS data analysis, Wentai
541 Chen and Yue Li for providing VOCs data.

544 **References**

- 545 Bond, T. C., Doherty, S. J., Fahey, D. W., Forster, P. M., Berntsen, T., DeAngelo, B. J., Flanner,
546 M. G., Ghan, S., Kärcher, B., Koch, D., Kinne, S., Kondo, Y., Quinn, P. K., Sarofim, M. C.,
547 Schultz, M. G., Schulz, M., Venkataraman, C., Zhang, H., Zhang, S., Bellouin, N.,
548 Guttikunda, S. K., Hopke, P. K., Jacobson, M. Z., Kaiser, J. W., Klimont, Z., Lohmann, U.,
549 Schwarz, J. P., Shindell, D., Storelvmo, T., Warren, S. G., and Zender, C. S.: Bounding the
550 role of black carbon in the climate system: A scientific assessment, *Journal of Geophysical*
551 *Research: Atmospheres*, 118, 5380-5552, doi:10.1002/jgrd.50171, 2013.
- 552 Canagaratna, M. R., Jimenez, J. L., Kroll, J. H., Chen, Q., Kessler, S. H., Massoli, P.,
553 Hildebrandt Ruiz, L., Fortner, E., Williams, L. R., Wilson, K. R., Surratt, J. D., Donahue,
554 N. M., Jayne, J. T., and Worsnop, D. R.: Elemental ratio measurements of organic
555 compounds using aerosol mass spectrometry: characterization, improved calibration, and
556 implications, *Atmos. Chem. Phys.*, 15, 253-272, doi:10.5194/acp-15-253-2015, 2015.
- 557 Claeys, M.: Formation of Secondary Organic Aerosols Through Photooxidation of Isoprene,
558 *Science*, 303, 1173-1176, doi:10.1126/science.1092805, 2004.
- 559 DeCarlo, P. F., Slowik, J. G., Worsnop, D. R., Davidovits, P., and Jimenez, J. L.: Particle
560 Morphology and Density Characterization by Combined Mobility and Aerodynamic
561 Diameter Measurements. Part 1: Theory, *Aerosol Sci. Tech.*, 38, 1185-1205,
562 10.1080/027868290903907, 2004.
- 563 DeCarlo, P. F., Kimmel, J. R., Trimborn, A., Northway, M. J., Jayne, J. T., Aiken, A. C., Gonin,
564 M., Fuhrer, K., Horvath, T., Docherty, K. S., Worsnop, D. R., and Jimenez, J. L.: Field-
565 deployable, high-resolution, time-of-flight aerosol mass spectrometer, *Anal. Chem.*, 78,
566 8281-8289, doi:10.1021/ac061249n, 2006.
- 567 DeCarlo, P. F., Ulbrich, I. M., Crounse, J., de Foy, B., Dunlea, E. J., Aiken, A. C., Knapp, D.,
568 Weinheimer, A. J., Campos, T., Wennberg, P. O., and Jimenez, J. L.: Investigation of the
569 sources and processing of organic aerosol over the Central Mexican Plateau from aircraft
570 measurements during MILAGRO, *Atmos. Chem. Phys.*, 10, 5257-5280, doi:10.5194/acp-
571 10-5257-2010, 2010.
- 572 Ervens, B., Turpin, B. J., and Weber, R. J.: Secondary organic aerosol formation in cloud
573 droplets and aqueous particles (aqSOA): a review of laboratory, field and model studies,
574 *Atmos. Chem. Phys.*, 11, 11069-11102, doi:10.5194/acp-11-11069-2011, 2011.
- 575 Fortner, E. C., Zhao, J., and Zhang, R. Y.: Development of ion drift-chemical ionization mass
576 spectrometry, *Anal. Chem.*, 76, 5436-5440, doi:10.1021/ac0493222, 2004.
- 577 Gunthe, S. S., Rose, D., Su, H., Garland, R. M., Achtert, P., Nowak, A., Wiedensohler, A.,
578 Kuwata, M., Takegawa, N., Kondo, Y., Hu, M., Shao, M., Zhu, T., Andreae, M. O., and
579 Pöschl, U.: Cloud condensation nuclei (CCN) from fresh and aged air pollution in the
580 megacity region of Beijing, *Atmos. Chem. Phys.*, 11, 11023-11039, doi:10.5194/acp-11-
581 11023-2011, 2011.
- 582 Guo, S., Hu, M., Lin, Y., Gomez-Hernandez, M., Zamora, M. L., Peng, J. F., Collins, D. R.,
583 and Zhang, R. Y.: OH-Initiated Oxidation of m-Xylene on Black Carbon Aging, *Environ.*
584 *Sci. Technol.*, 50, 8605-8612, doi:10.1021/acs.est.6b01272, 2016.
- 585 Guo, S., Hu, M., Wang, Z. B., Slanina, J., and Zhao, Y. L.: Size-resolved aerosol water-soluble
586 ionic compositions in the summer of Beijing: implication of regional secondary formation,
587 *Atmos. Chem. Phys.*, 10, 947-959, 2010.

588 Guo, S., Hu, M., Zamora, M. L., Peng, J., Shang, D., Zheng, J., Du, Z., Wu, Z., Shao, M., Zeng,
589 L., Molina, M. J., and Zhang, R.: Elucidating severe urban haze formation in China, *P. Natl.*
590 *Acad. Sci. USA*, 111, 17373-17378, doi:10.1073/pnas.1419604111, 2014.

591 He, L.-Y., X.-F. Huang, L. Xue, M. Hu, Y. Lin, J. Zheng, R. Zhang, and Y.-H. Zhang:
592 Submicron aerosol analysis and organic source apportionment in an urban atmosphere in
593 Pearl River Delta of China using high-resolution aerosol mass spectrometry, *J. Geophys.*
594 *Res.* 116, D12304, doi:10.1029/2010JD014566, 2011.

595 Hu, M., Peng, J., Sun, K., Yue, D., Guo, S., Wiedensohler, A., and Wu, Z.: Estimation of Size-
596 Resolved Ambient Particle Density Based on the Measurement of Aerosol Number, Mass,
597 and Chemical Size Distributions in the Winter in Beijing, *Environ. Sci. Technol.*, 46, 9941-
598 9947, doi:10.1021/es204073t, 2012.

599 Hu, W., Hu, M., Hu, W., Jimenez, J. L., Yuan, B., Chen, W., Wang, M., Wu, Y., Chen, C., Wang,
600 Z., Peng, J., Zeng, L., and Shao, M.: Chemical composition, sources and aging process of
601 sub-micron aerosols in Beijing: contrast between summer and winter, *J. Geophys. Res.-*
602 *Atmos.*, 121, 1955-1977 doi:10.1002/2015jd024020, 2016.

603 Huang, X. F., He, L. Y., Hu, M., Canagaratna, M. R., Sun, Y., Zhang, Q., Zhu, T., Xue, L., Zeng,
604 L. W., Liu, X. G., Zhang, Y. H., Jayne, J. T., Ng, N. L., and Worsnop, D. R.: Highly time-
605 resolved chemical characterization of atmospheric submicron particles during 2008 Beijing
606 Olympic Games using an Aerodyne High-Resolution Aerosol Mass Spectrometer, *Atmos.*
607 *Chem. Phys.*, 10, 8933-8945, doi:10.5194/acp-10-8933-2010, 2010.

608 Intergovernmental Panel on Climate Change (IPCC), *Climate Change 2013: The Physical*
609 *Science Basis*, Cambridge Univ. Press, Cambridge, UK, 2013.

610 Jacobson, M. Z.: Strong radiative heating due to the mixing state of black carbon in
611 atmospheric aerosols, *Nature*, 409, 695-697, doi:10.1038/35055518, 2001.

612 Jimenez, J. L., Canagaratna, M. R., Donahue, N. M., Prevot, A. S. H., Zhang, Q., Kroll, J. H.,
613 DeCarlo, P. F., Allan, J. D., Coe, H., Ng, N. L., Aiken, A. C., Docherty, K. S., Ulbrich, I.
614 M., Grieshop, A. P., Robinson, A. L., Duplissy, J., Smith, J. D., Wilson, K. R., Lanz, V. A.,
615 Hueglin, C., Sun, Y. L., Tian, J., Laaksonen, A., Raatikainen, T., Rautiainen, J., Vaattovaara,
616 P., Ehn, M., Kulmala, M., Tomlinson, J. M., Collins, D. R., Cubison, M. J., Dunlea, J.,
617 Huffman, J. A., Onasch, T. B., Alfarra, M. R., Williams, P. I., Bower, K., Kondo, Y.,
618 Schneider, J., Drewnick, F., Borrmann, S., Weimer, S., Demerjian, K., Salcedo, D., Cottrell,
619 L., Griffin, R., Takami, A., Miyoshi, T., Hatakeyama, S., Shimono, A., Sun, J. Y., Zhang, Y.
620 M., Dzepina, K., Kimmel, J. R., Sueper, D., Jayne, J. T., Herndon, S. C., Trimborn, A. M.,
621 Williams, L. R., Wood, E. C., Middlebrook, A. M., Kolb, C. E., Baltensperger, U., and
622 Worsnop, D. R.: Evolution of Organic Aerosols in the Atmosphere, *Science*, 326, 1525-
623 1529, doi:10.1126/science.1180353, 2009.

624 Kalberer, M.: Identification of Polymers as Major Components of Atmospheric Organic
625 Aerosols, *Science*, 303, 1659-1662, doi:10.1126/science.1092185, 2004.

626 Khalizov, A. F., Xue, H., and Zhang, R.: Enhanced light absorption and scattering by carbon
627 soot aerosols internally mixed with sulfuric acid, *J. Phys. Chem.*, 113, 1066-1074,
628 doi:10.1021/jp807531n, 2009.

629 Khalizov, A. F., Zhang, R., Zhang, D., Xue, H., Pagels, J., and McMurry, P. H.: Formation of
630 highly hygroscopic soot aerosols upon internal mixing with sulfuric acid vapor, *J. Geophys.*
631 *Res.*, 114, doi:10.1029/2008jd010595, 2009.

- 632 Khalizov, A. F., Lin, Y., Qiu, C., Guo, S., Collins, D., and Zhang, R.: Role of OH-Initiated
633 Oxidation of Isoprene in Aging of Combustion Soot, *Environ. Sci. Technol.*, 47, 2254-2263,
634 doi:10.1021/es3045339, 2013.
- 635 Kuwata, M., Kondo, Y., Mochida, M., Takegawa, N., and Kawamura, K.: Dependence of CCN
636 activity of less volatile particles on the amount of coating observed in Tokyo, *J. Geophys.*
637 *Res.*, 112, doi:10.1029/2006jd007758, 2007.
- 638 Liu, S., Aiken, A. C., Gorkowski, K., Dubey, M. K., Cappa, C. D., Williams, L. R., Herndon,
639 S. C., Massoli, P., Fortner, E. C., Chhabra, P. S., Brooks, W. A., Onasch, T. B., Jayne, J. T.,
640 Worsnop, D. R., China, S., Sharma, N., Mazzoleni, C., Xu, L., Ng, N. L., Liu, D., Allan, J.
641 D., Lee, J. D., Fleming, Z. L., Mohr, C., Zotter, P., Szidat, S., and Prevot, A. S. H.: Enhanced
642 light absorption by mixed source black and brown carbon particles in UK winter, *Nat.*
643 *Commun.*, 6, Artn 8435, doi:10.1038/Ncomms9435, 2015.
- 644 Liu, Y., Shao, M., Fu, L. L., Lu, S. H., Zeng, L. M., and Tang, D. G.: Source profiles of volatile
645 organic compounds (VOCs) measured in China: Part I, Atmospheric Environment, 42,
646 6247-6260, doi:10.1016/j.atmosenv.2008.01.070, 2008.
- 647 Ma, Y., Brooks, S. D., Vidaurre, G., Khalizov, A. F., Wang, L., and Zhang, R.: Rapid
648 modification of cloud-nucleating ability of aerosols by biogenic emissions, *Geophys. Res.*
649 *Lett.*, 40, 6293-6297, doi:10.1002/2013gl057895, 2013.
- 650 Martin, M., Tritscher, T., Jurányi, Z., Heringa, M. F., Sierau, B., Weingartner, E., Chirico, R.,
651 Gysel, M., Prévôt, A. S. H., Baltensperger, U., and Lohmann, U.: Hygroscopic properties
652 of fresh and aged wood burning particles, *J. Aerosol Sci.*, 56, 15-29,
653 doi:10.1016/j.jaerosci.2012.08.006, 2013.
- 654 Moffet, R., Massoli, P., Lambe, A. T., Ahern, A. T., Williams, L. R., Ehn, M., Mikkilä, J.,
655 Canagaratna, M. R., Brune, W. H., Onasch, T. B., Jayne, J. T., Petäjä, T., Kulmala, M.,
656 Laaksonen, A., Kolb, C. E., Davidovits, P., Worsnop, D. R.: Relationship between aerosol
657 oxidation level and hygroscopic properties of laboratory generated secondary organic
658 aerosol (SOA) particles. Geophys. Res. Lett., 37, L24801, doi:10.1029/2010GL045258,
659 2010.Moffet, R. C., and Prather, K. A.: In-situ measurements of the mixing state and optical
660 properties of soot with implications for radiative forcing estimates, P. Natl. Acad. Sci. USA,
661 106, 11872-11877, doi:10.1073/pnas.0900040106, 2009.
- 662 Pagels, J., McMurry, P.H., Khalizov, A.F., and Zhang, R.: Processing of soot by controlled
663 sulphuric acid and water condensation—Mass and mobility relationship, *Aerosol Sci. Tech.*
664 43, 629–640, 2009.
- 665 Peng, J., Hu, M., Du, Z., Wang, Y., Zheng, J., Zhang, W., Yang, Y., Qin, Y., Zheng, R., Xiao,
666 Y., Wu, Y., Lu, S., Wu, Z., Guo, S., Mao, H., and Shuai, S.: Gasoline aromatic: a critical
667 determinant of urban secondary organic aerosol formation, *Atmos. Chem. Phys. Discuss.*,
668 doi:10.5194/acp-2017-254, in review, 2017.
- 669 Peng, J. F., Hu, M., Guo, S., Du, Z. F., Zheng, J., Shang, D. J., Zamora, M. L., Zeng, L. M.,
670 Shao, M., Wu, Y. S., Zheng, J., Wang, Y., Glen, C. R., Collins, D. R., Molina, M. J., and
671 Zhang, R. Y.: Markedly enhanced absorption and direct radiative forcing of black carbon
672 under polluted urban environments, *P. Natl. Acad. Sci. USA*, 113, 4266-4271,
673 doi:10.1073/pnas.1602310113, 2016.
- 674 Peng, J. F., Hu, M., Wang, Z. B., Huang, X. F., Kumar, P., Wu, Z. J., Guo, S., Yue, D. L., Shang,
675 D. J., Zheng, Z., and He, L. Y.: Submicron aerosols at thirteen diversified sites in China:

676 size distribution, new particle formation and corresponding contribution to cloud
677 condensation nuclei production, *Atmos. Chem. Phys.*, 14, 10249-10265, doi:10.5194/acp-
678 14-10249-2014, 2014.

679 Petters, M. D., and Kreidenweis, S. M.: A single parameter representation of hygroscopic
680 growth and cloud condensation nucleus activity, *Atmos. Chem. Phys.*, 7, 1961-1971, 2007.

681 [Petters, M. D., and Kreidenweis, S. M.: A single parameter representation of hygroscopic](#)
682 [growth and cloud condensation nucleus activity—Part 2: Including solubility, *Atmos. Chem.*](#)
683 [*Phys.*, 8, 6273– 6279, 2008.](#)

684 Qiu, C., Khalizov, A. F., and Zhang, R. Y.: Soot Aging from OH-Initiated Oxidation of Toluene,
685 *Environ. Sci. Technol.*, 46, 9464-9472, doi:10.1021/Es301883y, 2012.

686 Qiu, C., and Zhang, R.: Multiphase chemistry of atmospheric amines, *Phys. Chem. Chem. Phys.*
687 15, doi:10.1039/C3CP43446J, 5738-5752, 2013.

688 Reed, R. C.: Observations of secondary organic aerosol production and soot aging under
689 atmospheric conditions using a novel new environmental aerosol chamber, PhD dissertation,
690 Texas A&M Univ, College Station, TX., 2010.

691 Ruehl, C. R., Davies, J. F., and Wilson, K. R.: An interfacial mechanism for cloud droplet
692 formation on organic aerosols, *Science*, 351, 1447-1450, doi:10.1126/science.aad4889,
693 2016.

694 Saathoff, H., Naumann, K. H., Schnaiter, M., Schöck, W., Möhler, O., Schurath, U.,
695 Weingartner, E., Gysel, M., and Baltensperger, U.: Coating of soot and (NH₄)₂SO₄
696 particles by ozonolysis products of α -pinene, *J. Aerosol Sci.*, 34, 1297-1321,
697 doi:10.1016/s0021-8502(03)00364-1, 2003.

698 Santoro, R. J., Semerjian, H. G., and Dobbins, R. A.: Soot Particle Measurements in Diffusion
699 Flames, *Combust. Flame*, 51, 203-218, 1983.

700 Swietlicki, E., Hansson, H. C., HäMeri, K., Svenningsson, B., Massling, A., McFiggans, G.,
701 McMurry, P. H., PetÄJÄ, T., Tunved, P., Gysel, M., Topping, D., Weingartner, E.,
702 Baltensperger, U., Rissler, J., Wiedensohler, A., and Kulmala, M.: Hygroscopic properties
703 of submicrometer atmospheric aerosol particles measured with H-TDMA instruments in
704 various environments—a review, *Tellus B*, 60, 432-469, doi:10.1111/j.1600-
705 0889.2008.00350.x, 2008.

706 Tritscher, T., Jurányi, Z., Martin, M., Chirico, R., Gysel, M., Heringa, M. F., DeCarlo, P. F.,
707 Sierau, B., Prévôt, A. S. H., Weingartner, E., and Baltensperger, U.: Changes of
708 hygroscopicity and morphology during ageing of diesel soot, *Environ. Res. Lett.*, 6, 034026,
709 doi:10.1088/1748-9326/6/3/034026, 2011.

710 Wang, G. H., Zhang, R. Y., Gomez, M. E., Yang, L. X., Zamora, M. L., Hu, M., Lin, Y., Peng,
711 J. F., Guo, S., Meng, J. J., Li, J. J., Cheng, C. L., Hu, T. F., Ren, Y. Q., Wang, Y. S., Gao, J.,
712 Cao, J. J., An, Z. S., Zhou, W. J., Li, G. H., Wang, J. Y., Tian, P. F., Marrero-Ortiz, W.,
713 Secrest, J., Du, Z. F., Zheng, J., Shang, D. J., Zeng, L. M., Shao, M., Wang, W. G., Huang,
714 Y., Wang, Y., Zhu, Y. J., Li, Y. X., Hu, J. X., Pan, B., Cai, L., Cheng, Y. T., Ji, Y. M., Zhang,
715 F., Rosenfeld, D., Liss, P. S., Duce, R. A., Kolb, C. E., and Molina, M. J.: Persistent sulfate
716 formation from London Fog to Chinese haze, *P. Natl. Acad. Sci. USA*, 113, 13630-13635,
717 doi:10.1073/pnas.1616540113, 2016.

718 Wang, L., Khalizov, A. F., Zheng, J., Xu, W., Ma, Y., Lal, V., and Zhang, R. Y.: Atmospheric
719 nanoparticles formed from heterogeneous reactions of organics, *Nat. Geosci.*, 3, 238-242,

720 doi:10.1038/NGEO778, 2010.

721 Wang, Y., Wan, Q., Meng, W., Liao, F., Tan, H., and Zhang, R.: Long-term impacts of aerosols
722 on precipitation and lightning over the Pearl River Delta megacity area in China, *Atmos.*
723 *Chem. Phys.* 11, 12421–12436, 2011.

724 Wang, Y., Khalizov, A., Levy, M., and Zhang, R.: Light absorbing aerosols and their
725 atmospheric impacts, *Atmos. Environ.* 81, 713-715, doi:10.1016/j.atmosenv.2013.09.034,
726 2013.

727 Weingartner, E., Burtscher, H., and Baltensperger, U.: Hygroscopic properties of carbon and
728 diesel soot particles, *Atmos. Environ.*, 31, 2311-2327, doi:10.1016/S1352-2310(97)00023-
729 X, 1997.

730 Wittbom, C., Eriksson, A. C., Rissler, J., Carlsson, J. E., Roldin, P., Nordin, E. Z., Nilsson, P.
731 T., Swietlicki, E., Pagels, J. H., and Svenningsson, B.: Cloud droplet activity changes of
732 soot aerosol upon smog chamber ageing, *Atmos. Chem. Phys.*, 14, 9831-9854,
733 doi:10.5194/acp-14-9831-2014, 2014.

734 Wu, Z. J., Zheng, J., Shang, D. J., Du, Z. F., Wu, Y. S., Zeng, L. M., Wiedensohler, A., and Hu,
735 M.: Particle hygroscopicity and its link to chemical composition in the urban atmosphere
736 of Beijing, China, during summertime, *Atmos. Chem. Phys.*, 16, 1123-1138,
737 doi:10.5194/acp-16-1123-2016, 2016.

738 Xue, H., Khalizov, A. F., Wang, L., Zheng, J., and Zhang, R.: Effects of dicarboxylic acid
739 coating on the optical properties of soot, *Phys. Chem. Chem. Phys.*, 11, 7865-7875,
740 doi:10.1039/b700001a, 2009a.

741 Xue, H., Khalizov, A. F., and Zhang, R.: Effects of coating of dicarboxylic acids on the mass-
742 mobility relationship of soot particles, *Environ. Sci. Technol.* 43, 2787–2792, doi:
743 10.1021/es803287v, 2009b.

744 Yuan, T., Li, Z., Zhang, R., and Fan, J.: Increase of cloud droplet size with aerosol optical depth:
745 An observation and modeling study, *J. Geophys. Res.*, 113, D04201,
746 doi:10.1029/2007JD008632, 2008.

747 Zhang, D., and Zhang R.: Laboratory investigation of heterogeneous interaction of sulfuric
748 acid with soot, *Environ. Sci. Technol.* 39, 5722-5727, doi:10.1021/es050372d, 2005.

749 Zhang, R., Khalizov, A. F., Pagels, J., Zhang, D., Xue, H., and McMurry, P. H.: Variability in
750 morphology, hygroscopicity, and optical properties of soot aerosols during atmospheric
751 processing, *P. Natl. Acad. Sci. USA*, 105, 10291-10296, doi:10.1073/pnas.0804860105,
752 2008.

753 Zhang, R. Y., Suh, I., Zhao, J., Zhang, D., Fortner, E. C., Tie, X. X., Molina, L. T., and Molina,
754 M. J.: Atmospheric new particle formation enhanced by organic acids, *Science*, 304, 1487-
755 1490, doi:10.1126/science.1095139, 2004.

756 Zhang, R., Khalizov, A.F., Wang, L., Hu, M., Xu, W.: Nucleation and growth of nanoparticles
757 in the atmosphere, *Chem. Rev.*, 112, 1957-2011, doi:10.1021/cr2001756, 2012.

758 Zhang, R. Y., Wang, G. H., Guo, S., Zarnora, M. L., Ying, Q., Lin, Y., Wang, W. G., Hu, M.,
759 and Wang, Y.: Formation of Urban Fine Particulate Matter, *Chem. Rev.*, 115, 3803-3855,
760 doi:10.1021/acs.chemrev.5b00067, 2015.

761 Zhao, J., Levitt, N. P., Zhang, R., and Chen, J.: Heterogeneous reactions of methylglyoxal in
762 acidic media: Implications for secondary organic aerosol formation, *Environ. Sci. Technol.*,
763 40, 7682-7687, doi:10.1021/es060610k, 2006.

-
- 764 Zhao, J., Khalizov, A.F., Zhang, R., and McGraw, R.: Hydrogen bonding interaction of
765 molecular complexes and clusters of aerosol nucleation precursors, *J. Phys. Chem.*, 113,
766 680–689, doi:10.1021/jp806693r, 2009.
- 767 Zhao, P. S., Dong, F., He, D., Zhao, X. J., Zhang, X. L., Zhang, W. Z., Yao, Q., and Liu, H. Y.:
768 Characteristics of concentrations and chemical compositions for PM_{2.5} in the region of
769 Beijing, Tianjin, and Hebei, China, *Atmos. Chem. Phys.*, 13, 4631-4644, doi:10.5194/acp-
770 13-4631-2013, 2013.
- 771 Zheng, J., Zhang, R., Fortner, E. C., Volkamer, R. M., Molina, L., Aiken, A. C., Jimenez, J. L.,
772 Gaeggeler, K., Dommen, J., Dusanter, S., Stevens, P.S., and Tie, X.: Measurements of
773 HNO₃ and N₂O₅ using ion drift - chemical ionization mass spectrometry during the MCMA
774 - 2006 campaign, *Atmos. Chem. Phys.*, 8, 6823–6838, 2008.
- 775 Zheng, J., Khalizov, A., Wang, L., and Zhang, R. Y.: Atmospheric Pressure-Ion Drift Chemical
776 Ionization Mass Spectrometry for Detection of Trace Gas Species, *Anal. Chem.*, 82, 7302-
777 7308, doi:10.1021/ac101253n, 2010.

Table 1. Summary of ambient conditions for BC aging experiments conducted in Beijing. The PM_{2.5}, gas concentrations and meteorological condition were averaged from the entire experimental time. D_m and T represent the mobility diameter and temperature, respectively.

No.	Date	Time		Initial D _m (nm)	PM _{2.5} (μg m ⁻³)	J(O ¹ D) (10 ⁻⁶)	Gas Concentration (ppb)					Meteorological Conditions	
		Start	End				Toluene	Xylene	SO ₂	NO _x	O ₃	T (°C)	RH (%)
#1	Aug. 18 th	12:41	14:47	95	43	19	0.49	0.13	1.7	8.8	56	35	27
#2	Aug. 22 nd	13:32	16:51	96	69	3.7	3.41	0.78	2	36.1	26	26	69
#3	Sep. 7 th	12:40	14:52	97	12	17.5	0.71	0.17	2.7	10.2	75	30	35
#4	Sep. 9 th	13:13	17:06	97	40	6.3	0.77	0.21	4	11	68	26	50
#5	Sep. 1 st	13:19	16:13	147	27	11.6	0.76	0.19	4.6	19.9	83	31	33
#6	Sep. 11 st	13:50	17:25	147	57	6.1	1.57	0.39	6.7	17.1	92	29	42
#7	Sep. 21 st	15:31	17:41	146	30	2.1	0.75	0.29	2	10.6	90	28	37
#8	Aug. 24 th	11:37	16:06	216	8.8	21.1	0.98	0.3	1.7	15.6	57	36	25
#9	Sep. 5 th	14:06	16:44	220	12	8.3	0.45	0.2	2.2	14.6	54	29	35
#10	Oct. 17 th	12:54	17:13	224	57	3.2	-	-	13.8	41	34	18	30

Table 2. Summary of particle properties for BC aging experiments conducted in Beijing. D_m , ρ_{eff} and D_{me} represent the mobility diameter, effective density and mass equivalent diameter, respectively.

No.	Date	D_m		ρ_{eff}		D_{me}		ΔD_{me} (nm)	Growth Rate ^a (nm h ⁻¹)
		Initial (nm)	Final (nm)	Initial (g cm ⁻³)	Final (g cm ⁻³)	Initial (nm)	Final (nm)		
#1	Aug. 18 th	95	157	0.50	1.35	62	162	100	47
#2	Aug. 22 nd	96	129	0.46	1.31	61	126	65	20
#3	Sep. 7 th	97	147	0.45	1.25	62	142	80	36
#4	Sep. 9 th	97	136	0.43	1.30	61	133	62	19
#5	Sep. 1 st	147	170	0.34	1.36	85	168	83	29
#6	Sep. 11 st	147	162	0.34	1.34	84	159	75	20
#7	Sep. 21 st	146	132	0.34	1.05	84	116	32	15
#8	Aug. 24 th	216	272	0.32	1.37	123	275	152	34
#9	Sep. 5 th	220	202	0.25	1.33	114	197	83	31
#10	Oct. 17 th	224	224	0.24	0.52	117	157	40	11
Average								77 ± 33	26 ± 11

^a The growth rate is calculated using the data between 12:00 and 17:00 for each experiment.

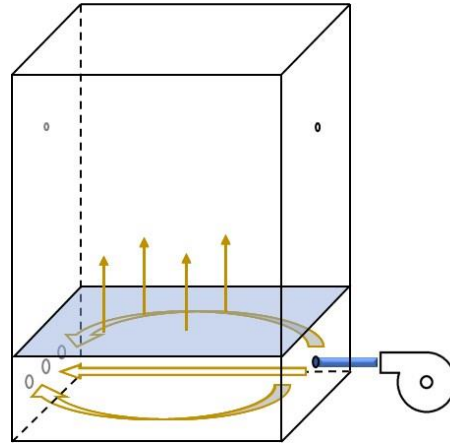


Figure 1. Photo (left) and schematic (right) of the quasi-atmospheric aerosol evolution study (QUALITY) chamber

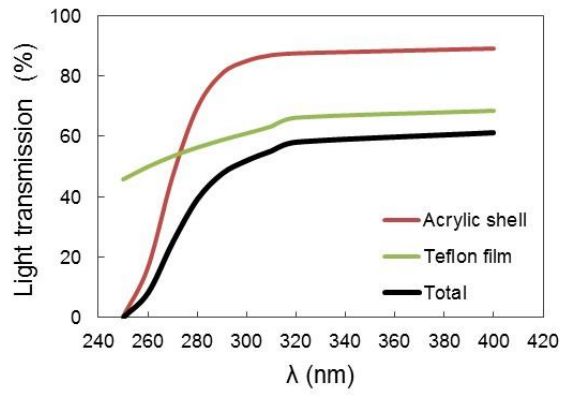


Figure 2. Light transmission spectra of the PFA Teflon film (yellow line), the acrylic shell (red line), and their total transmission in the UV range (black line).

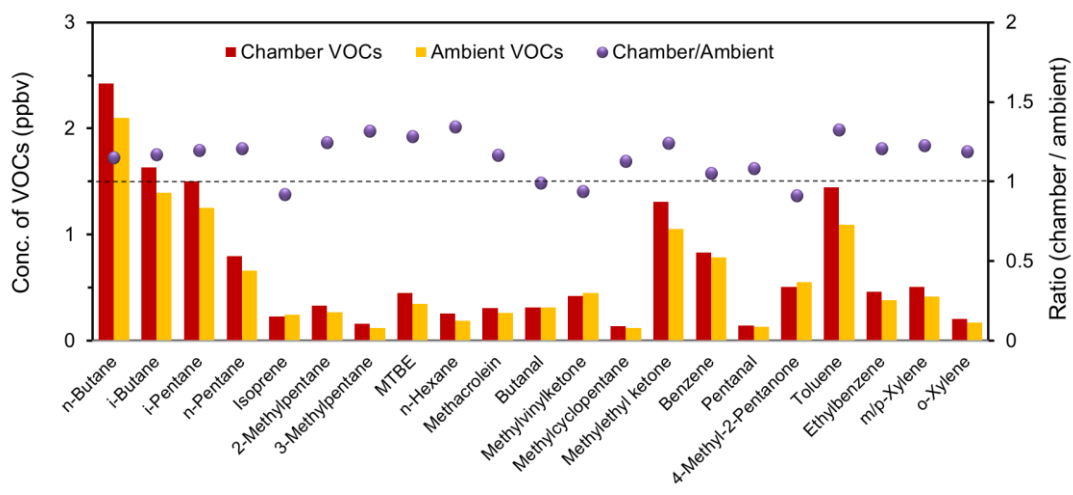


Figure 3. Comparison of VOCs concentrations in the QUALITY chamber (red bar) and in the ambient air (yellow bar) before the start of BC aging experiment. Purple cycles represent the ratio of each species in the reaction chamber to in the ambient air. Only the VOCs species that contains 4 or more carbons with the concentration higher than 0.1 ppb are shown in the figure.

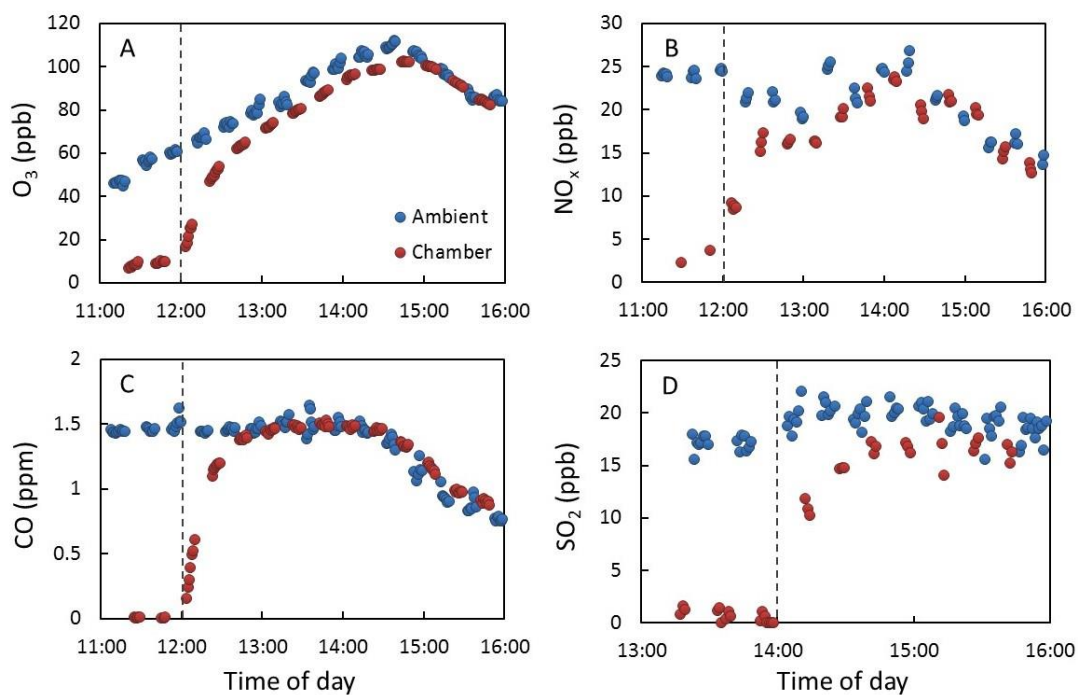


Figure 34. Concentrations of O_3 (A), NO_x (B), CO (C), and SO_2 (D) measured inside the QUALITY chamber (Red circles) and in the ambient air (blue circles). The vertical dashed lines denote the time when the ambient air started to be pulled through the bottom flow chamber and the ambient gases began to exchange into the upper reaction chamber.

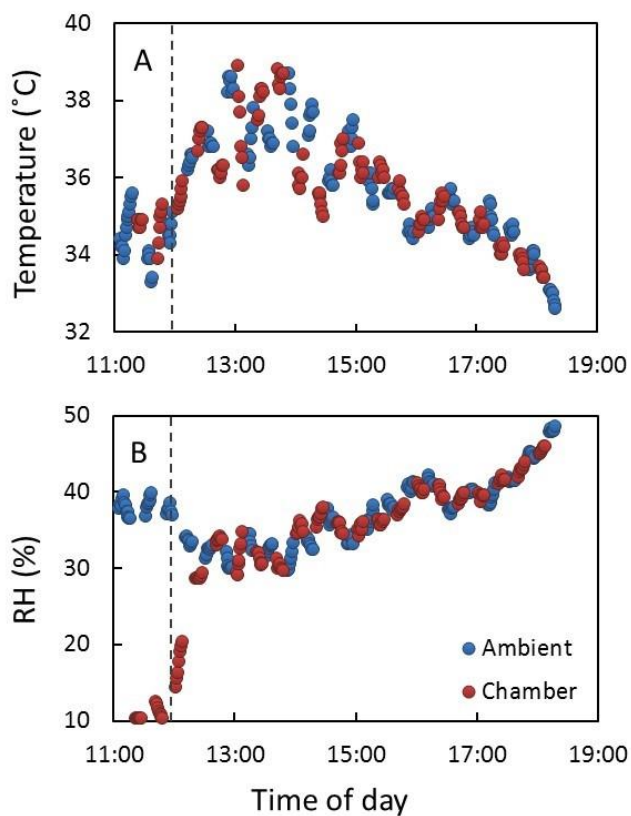


Figure 45. Temperature (A) and RH (B) measured inside the QUALITY chamber (Red circles) and in the ambient air (blue circles). The temperature and RH were measured by probes placed in the sampling tube adjacent to the chamber. The vertical dashed lines denote the time when the ambient air started to be pulled through the bottom flow chamber and the ambient gases began to exchange into the upper reaction chamber.

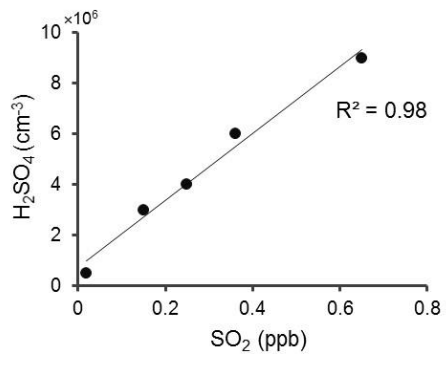
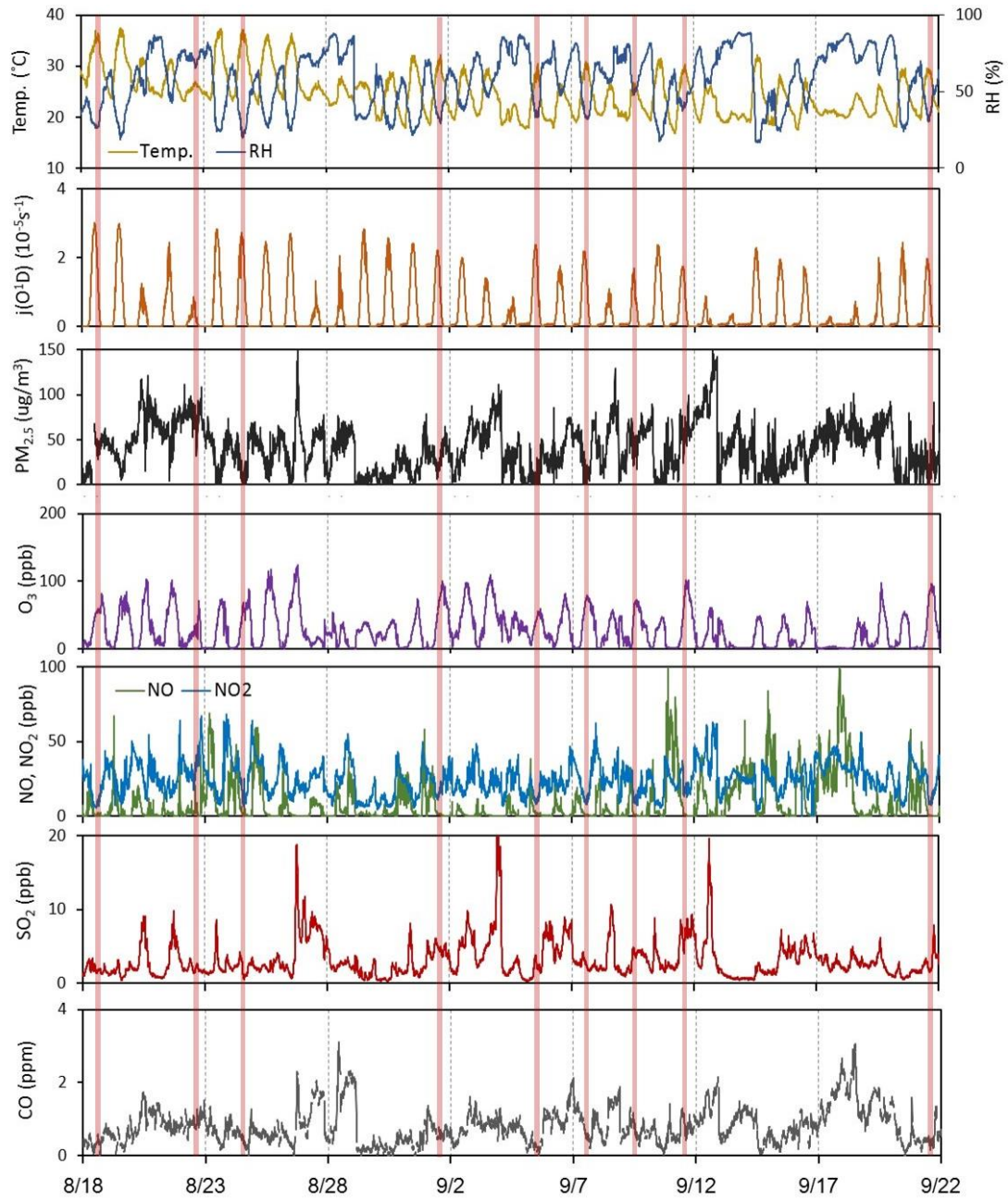


Figure 56. Sulfuric acid concentration as function of SO₂ concentration inside the chamber



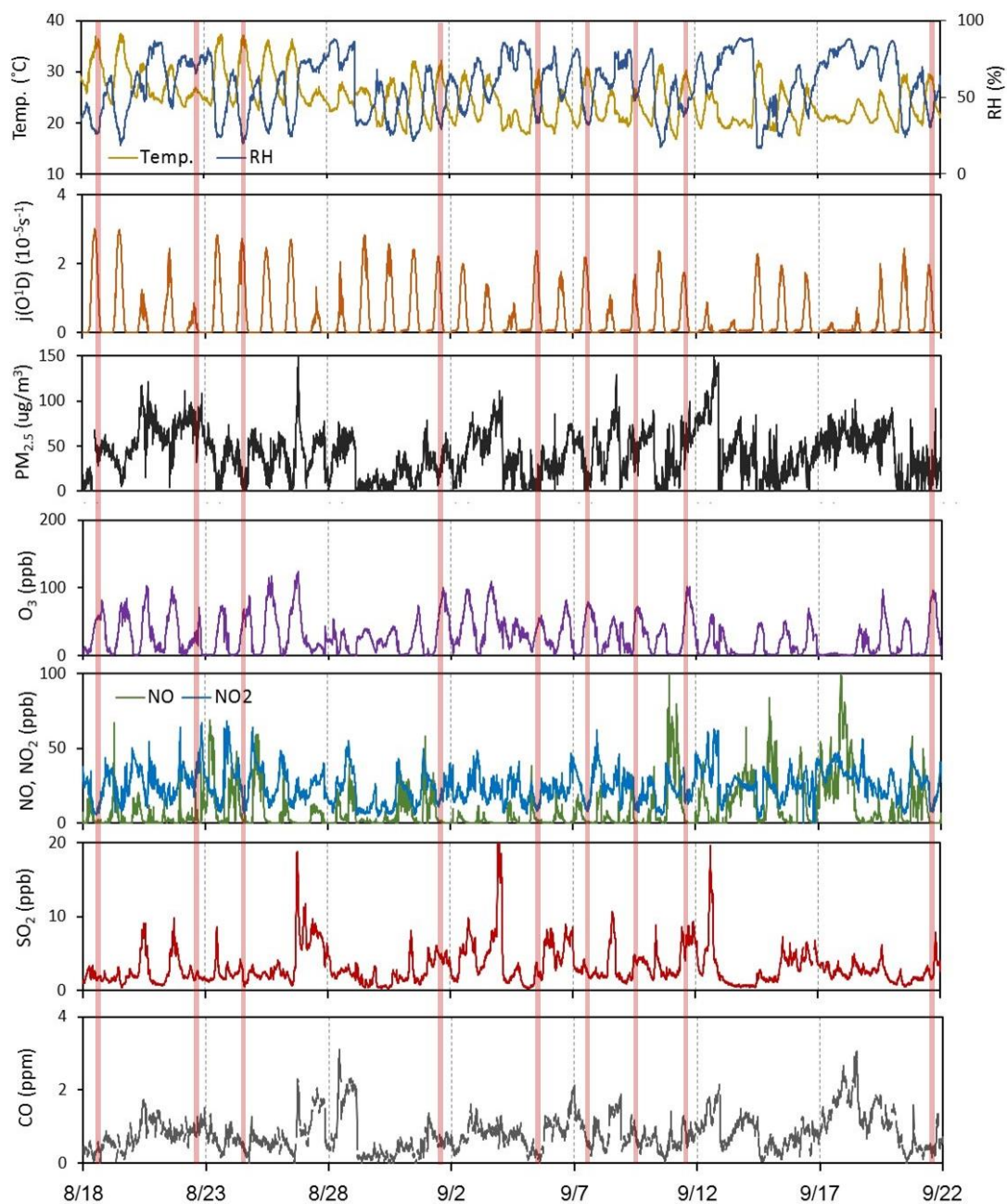


Figure 67. Time series of ambient pollutant concentrations and meteorological parameters during the experimental period in Beijing. Red bars indicate periods when BC aging experiments were conducted.

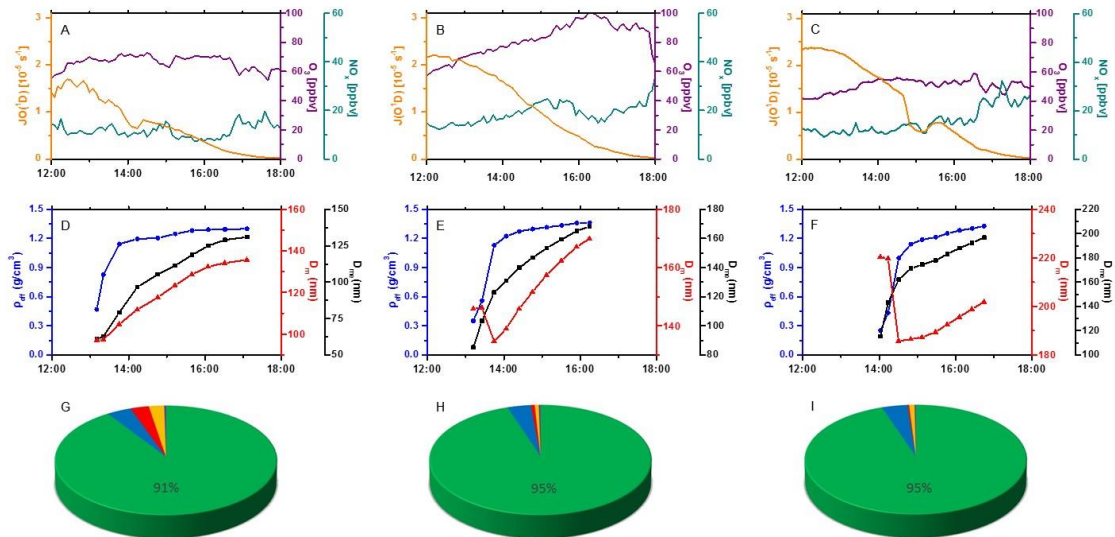


Figure 78. Ambient condition (A, B, C), changes of diameter and density of BC particle (D, E, F), and the chemical composition of coating materials (G, H, I) during three typical aging experiments. A and D correspond to experiment #4; B and E correspond to experiment #5, and C and E correspond to experiment #9. D_m is the peak mobility diameter of BC particles, ρ_{eff} is the best-fit effective density of BC particles with the mobility diameter D_m , D_{me} is the mass equivalent diameter of BC particles, and $J(O^1D)$ represents the measured photolysis rate constant for O^1D . The colors of green, blue, red, yellow and purple in the pie charts represent organics, nitrate, sulfate, ammonium, and chlorine, respectively. The numbers in figure G, H and I are the mass fraction of organics.

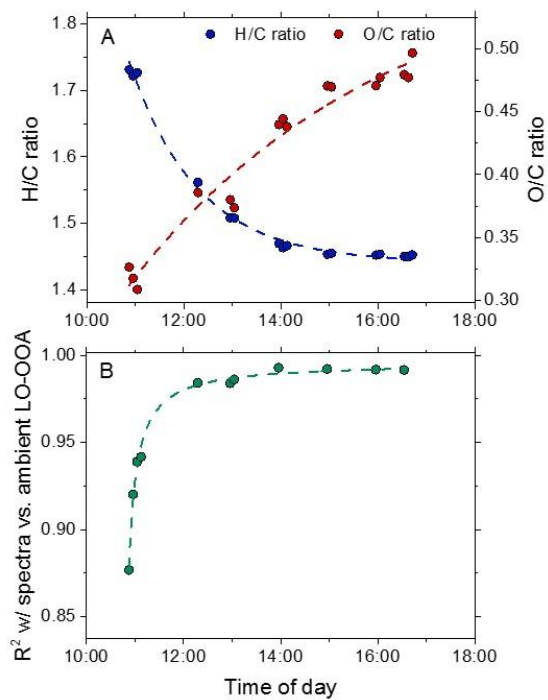


Figure 89. The evolution of organic aerosols inside the chamber during an aging experiment (#8) in Beijing. (A) the H/C and O/C ratios of organics on aged BC particles; (b) the correlation coefficients (R^2) between the evolving total OA spectra in chamber experiment and the LO-OOA spectra derived from the Beijing field data set.

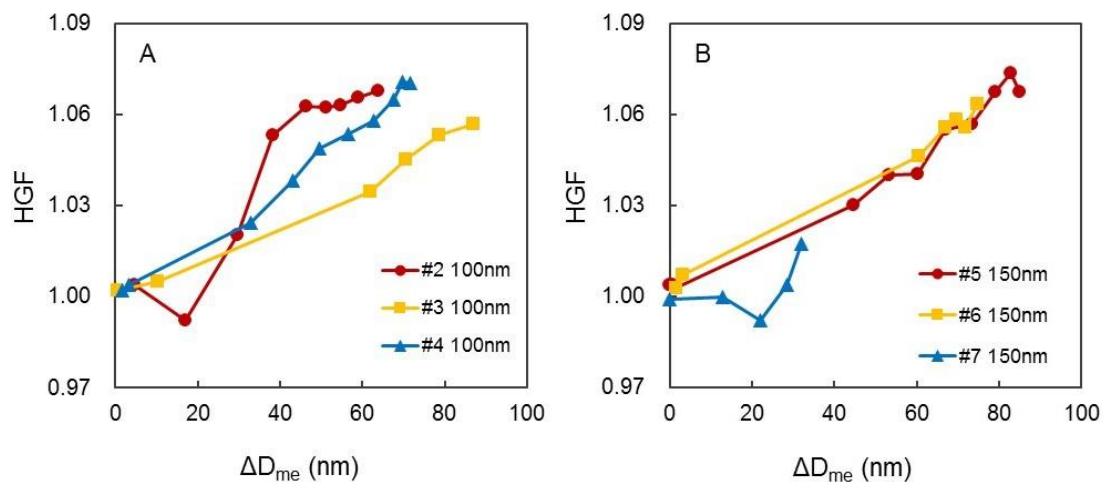


Figure 910. Evolution of hygroscopic growth factors (HGF) of BC particles during aging as a function of ΔD_{me} . (A) three experiments with 100 nm BC particle; (B) three experiments with 150 nm BC particle. Different colors in each figure represent different experiments. Hygroscopicity measurement is not available for experiment #1.

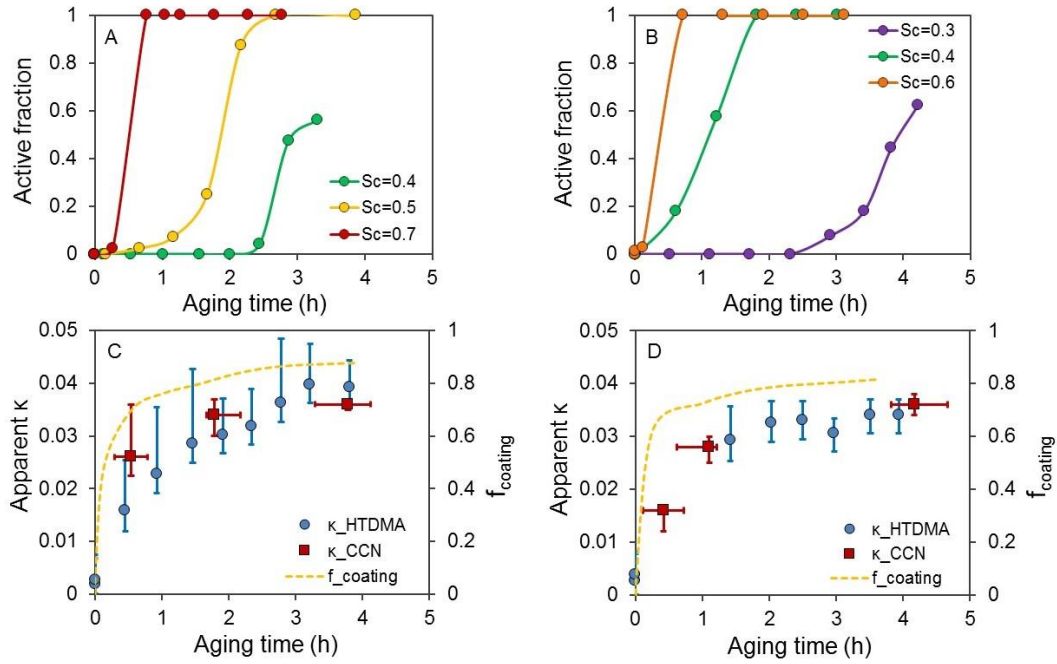


Figure 1011. The active fraction of BC particles under diversified supersaturation (A, B) and the closure of apparent κ for BC particles with initial diameter (C, D) during aging in two typical experiments. A, C are the results from experiment #4 with 100nm BC particles and B, D represents experiment #6 with 150nm BC particles. Red square and blue circle in C and D represent the apparent κ calculated using CCN counter data and HTDMA data, respectively. Yellow slash line represents the fraction of coating materials on BC particles. The error bars of κ_{CCN} and κ_{HTDMA} represent the uncertainty in the calculation.